UNIVERSIDAD DE CONCEPCIÓN

Centro de Investigación en Ingeniería Matemática (CI^{2}MA)

On the implementation of WENO schemes for a class of polydisperse sedimentation models

Raimund Bürger, Rosa Donat,
Pep Mulet, Carlos A. Vega

PREPRINT 2010-21

SERIE DE PRE-PUBLICACIONES

ON THE IMPLEMENTATION OF WENO SCHEMES FOR A CLASS OF POLYDISPERSE SEDIMENTATION MODELS

RAIMUND BÜRGER[A], ROSA DONAT[B], PEP MULET[B], AND CARLOS A. VEGA[C]

ABSTRACT. The sedimentation of a polydisperse suspension of small rigid spheres of the same density, but which belong to a finite number of species (size classes), can be described by a spatially one-dimensional system of first-order, nonlinear, strongly coupled conservation laws. The unknowns are the volume fractions (concentrations) of each species as functions of depth and time. Typical solutions, e.g. for batch settling in a column, include discontinuities (kinematic shocks) separating areas of different composition. The accurate numerical approximation of these solutions is a challenge since closed-form eigenvalues and eigenvectors of the flux Jacobian are usually not available, and the characteristic fields are neither genuinely nonlinear nor linearly degenerate. However, the flux vectors associated with the widely used models by Masliyah, Lockett and Bassoon (MLB model) and Höfler and Schwarzer (HS model) give rise to Jacobians that are low-rank perturbations of a diagonal matrix. This property allows to apply a convenient hyperbolicity criterion that has become known as the "secular equation" [J. Anderson, Lin. Alg. Appl. 246 (1996) 49–70]. This criterion was recently applied [R. Bürger, R. Donat, P. Mulet, C.A. Vega, SIAM J. Appl. Math. 70 (2010) 2186–2213] to prove that the MLB and HS models are strictly hyperbolic under easily verifiable conditions, that their eigenvalues interlace with the velocities of the species that form the flux vector (so the velocities are good starting values for a root finder), and that the corresponding eigenvectors can be calculated with acceptable effort. In the present work, the newly available characteristic information is exploited for the implementation of characteristic-wise (spectral) weighted essentially non-oscillatory (WENO) schemes for the MLB and HS models. Numerical examples illustrate that WENO schemes which use this spectral information are superior in resolution, and even in efficiency for the same overall resolution, to component-wise WENO schemes.

1. INTRODUCTION

1.1. **Scope.** This work concerns high-resolution numerical schemes for systems of conservation laws that arise as one-dimensional kinematic models for the sedimentation of polydisperse suspensions. These mixtures consist of small solid particles that belong to a number N of species that may differ in size or density, and which are dispersed in a viscous fluid. We will herein only consider particles of the same density. If ϕ_i denotes the volume fraction of particle species i having diameter D_i, where we assume that $D_1 > D_2 > \ldots > D_N$, and v_i is the phase velocity of species i, then the continuity equations of the N species are $\partial_t \phi_i + \partial_x(\phi_i v_i) = 0$, $i = 1, \ldots, N$, where t is time and x is depth. The velocities $v_1, \ldots, v_N$ are assumed to be given functions of the vector $\Phi := \Phi(x,t) := (\phi_1(x,t), \ldots, \phi_N(x,t))^{\mathrm{T}}$ of local concentrations. This yields nonlinear, strongly coupled systems of conservation laws of the type

$$\partial_t \Phi + \partial_x \mathbf{f}(\Phi) = 0, \quad \mathbf{f}(\Phi) := \big(f_1(\Phi), \ldots, f_N(\Phi)\big)^{\mathrm{T}}, \quad f_i(\Phi) := \phi_i v_i(\Phi), \quad i = 1, \ldots, N. \tag{1.1}$$

We seek solutions $\Phi = \Phi(x,t)$ that take values in $\Phi \in \bar{\mathcal{D}}_{\phi_{\max}} \subset \mathbb{R}^N$, where $\bar{\mathcal{D}}_{\phi_{\max}}$ is the closure of the set

$$\mathcal{D}_{\phi_{\max}} := \big\{\Phi \in \mathbb{R}^N \,:\, \phi_1 > 0, \ldots, \phi_N > 0,\, \phi := \phi_1 + \cdots + \phi_N < \phi_{\max}\big\}.$$

Date: October 21, 2010.

[A]CI^{2}MA and Departamento de Ingeniería Matemática, Facultad de Ciencias Físicas y Matemáticas, Universidad de Concepción, Casilla 160-C, Concepción, Chile. E-Mail: rburger@ing-mat.udec.cl.

[B]Departament de Matemàtica Aplicada, Universitat de València, Av. Dr. Moliner 50, E-46100 Burjassot, Spain. E-Mail: donat@uv.es, mulet@uv.es.

[C]Departamento de Ingeniería Matemática, Facultad de Ciencias Físicas y Matemáticas, Universidad de Concepción, Casilla 160-C, Concepción, Chile. Permanent address: Departamento de Matemáticas y Estadística, División de Ciencias Básicas, Universidad del Norte, Barranquilla, Colombia. E-Mail: cvega@uninorte.edu.co.

The parameter $0 < \phi_{\max} \leq 1$ stands for a given maximum solids concentration. For batch settling of a suspension in a column of height L, (1.1) is defined on $\Omega_T := \{(x,t) \in \mathbb{R}^2 \,|\, 0 \leq x \leq L,\ 0 \leq t \leq T\}$ for a given final time $T > 0$ along with the initial condition

$$\Phi(x,0) = \Phi^0(x) = \big(\phi_1^0(x), \ldots, \phi_N^0(x)\big)^{\mathrm{T}}, \quad \Phi^0(x) \in \bar{\mathcal{D}}_{\phi_{\max}}, \quad x \in [0,L] \tag{1.2}$$

and the zero-flux boundary conditions

$$\mathbf{f}|_{x=0} = \mathbf{f}|_{x=L} = 0. \tag{1.3}$$

Several choices of v_i ("models"), or equivalently, of the fluxes f_i, as functions of Φ, and depending on the vector of normalized particle sizes $\mathbf{d} := (d_1, \ldots, d_N)^{\mathrm{T}}$, where $d_i := D_i/D_1$ for $i = 1, \ldots, N$, have been proposed in the literature. We restrict ourselves to the two models due to Masliyah [30] and Lockett and Bassoon [29] ("MLB model") and Höfler and Schwarzer [10, 23, 24] ("HS model"), respectively. It was recently shown in [9] that both models are strictly hyperbolic for all $\Phi \in \mathcal{D}_{\phi_{\max}}$, for arbitrary N, and under easily verifiable, mild restrictions on certain model-specific parameters and the smallest normalized particle size d_N. The key structural property of both models, which led to these results, consists in that the fluxes f_i do not depend on each of the N components of Φ in an individual way, but only on a small number $m \ll N$ ($m = 2$ and $m = 3$ for the MLB and HS models, respectively) of scalar functions of Φ. Therefore, the Jacobian $\mathcal{J}_{\mathbf{f}}(\Phi)$ is a rank-m perturbation of a diagonal matrix. The analysis of [9] also provides sharp bounds of the eigenvalues of $\mathcal{J}_{\mathbf{f}}(\Phi)$. This information eventually permits us to numerically calculate the eigenvalues and corresponding eigenvectors of $\mathcal{J}_{\mathbf{f}}(\Phi)$ with acceptable effort. Numerical simulations with low-order schemes were presented in [9], but it was conjectured that this characteristic (or spectral) information could be employed advantageously for the implementation of high-resolution schemes.

It is the purpose of this work to demonstrate that very efficient high-order accurate weighted essentially non-oscillatory (WENO) schemes for the numerical solution of (1.1)–(1.3) can indeed be constructed by incorporating characteristic information related to (1.1). This information is available due to the recent hyperbolicity analysis made in [9], and can be incorporated in various ways. Specifically, we use the results in [9] in order to provide a good estimation of the viscosity coefficient in a Lax-Friedrichs-type flux splitting. This allows to construct high resolution component-wise WENO schemes, akin to those proposed in [44] for the Multiclass Lighthill-Whitham-Richards (MCLWR) models in traffic flow. In addition, the full spectral decomposition of $\mathcal{J}_{\mathbf{f}}(\Phi)$, which can be numerically computed at each cell interface thanks to the analysis in [9], can be used in order to obtain *characteristic-based* WENO schemes, for which the WENO reconstruction procedure is applied to the local characteristic variables and fluxes at each cell-interface. When combined with a a strong stability preserving (SSP) Runge-Kutta-type time discretization, the resulting SSP-WENO-SPEC schemes are shown to be extremely robust in a number of numerical experiments concerning the MLB and HS models, including several properties specific to the present application such as non-negativity of the solution, almost avoidance of overshoots of the numerical total density ϕ beyond $\phi_{\max}$, and accurate rendering of stationary kinematic shocks that separate sediment layers of different composition.

1.2. **Related work.** WENO-type spatial flux reconstructions, which emerged from earlier essentially non-oscillatory (ENO) schemes, have become a well-established, versatile tool for the construction of high-resolution conservative schemes in numerous applications. The first WENO scheme, of third-order accuracy, was introduced by Liu, Osher and Chan in [28], while a general framework to construct WENO schemes of arbitrary order of accuracy was provided by Jiang and Shu [25]. We refer to Shu [39, 40] for further details, applications, and references. If applied to a system of conservation laws, the WENO procedure will produce a spatially semi-discrete system of ODE, for which a discretization in time can be chosen separately [38]. A suitable choice are total variation diminishing Runge-Kutta schemes [20, 39], also known as strong stability preserving (SSP) methods [21], because of their favorable stability properties.

While WENO-based high-resolution shock-capturing schemes have been applied successfully to a wide range of convection-dominated problems [40], the polydisperse sedimentation models considered herein present some specific challenges for numerical simulation. These models belong to the wider class of multi-species kinematic flow models [13], which are characterized by a governing system of equations of the type (1.1) with explicit velocity functions $v_1, \ldots, v_N$ for a number N of species. Models of this type include, besides

the sedimentation model, a model of settling of oil-in-water dispersion [33] and, most notably, the multi-class Lighthill-Whitham-Richards (MCLWR) kinematic traffic model, which extends the well-known LWR model to vehicles with drivers having different preferential velocities, and which was proposed by Benzoni-Gavage and Colombo [5] and Wong and Wong [41]. Meanwhile, the MCLWR model has been studied thoroughly in a series of papers including [13, 42, 43, 44, 45]. All these models can be formulated for an arbitrary number N of species, that is, of scalar equations. The basic phenomenon of interest is the segregation of species, i.e. the formation of areas of different composition from an initially homogeneous "mixture" (e.g., suspension or traffic platoon). Segregation is usually associated with the formation of discontinuities in Φ, so-called kinematic shocks. For the sedimentation model considered for batch settling in a column, stationary kinematic shocks separate sediment layers of different composition. The accurate numerical simulation of the model is therefore of importance for the prediction of the composition of the sediment as a final "product" or deposit e.g. in medicine, the manufacturing of functionally graded materials, volcanology, and petrology (see e.g. [2] for references to these applications).

It is well known that high-resolution shock capturing schemes can be applied to systems of conservation laws either in a component-wise or in a characteristic-wise (spectral) fashion. The latter requires a detailed knowledge of the spectral decomposition of the Jacobian matrix of the system, since the eigenstructure is used in a fundamental way in the design principles of the scheme [17]. For multi-species kinematic flow models, however, eigenvalues are not available in closed form, nevertheless it has been possible to prove strict hyperbolicity of some of these models by an explicit representation of the characteristic polynomial [7, 33, 42], as well as to obtain an interlacing property of the (unknown) eigenvalues of the Jacobian $\lambda_1, \dots, \lambda_N$ with the (known) velocities $v_1, \dots, v_N$, which provide excellent starting values for a root finder. For the MCLWR model, the corresponding hyperbolicity and characteristic analysis was first done by Zhang et al. [43]. In [45], solutions to this model, with the additional complication of a discontinuously varying coefficient modeling variable road surface conditions, were compared with solutions generated by a component-wise WENO scheme which provides good overall accuracy. The first implementation of a component-wise WENO scheme for that model had been done by Zhang in [42], and pre-dates the hyperbolicity analysis in [43]. An improvement of the component-wise scheme in [43] is presented in [44], and used in subsequent papers. It amounts to using a more appropriate choice of the viscosity coefficient in a Lax-Friedrichs flux splitting, and is based on sharper bound for the smallest eigenvalue obtained from the hyperbolicity analysis of the MCLWR model carried out in [43]. We shall see that the results in [9] easily lead to an analogous estimation of the viscosity coefficient for the polydisperse sedimentation models considered in this paper.

The hyperbolicity analysis for the MCLWR model is, in fact, fairly straightforward since that model gives rise to a Jacobian which is a rank-1 perturbation of a diagonal (see Section 1.1). In [17], this feature was exploited in order to give a much simpler proof of the hyperbolicity of the MCLWR model. The full spectral decomposition of the Jacobian matrix was then used to construct a characteristic-based version of the schemes utilized in [42], and it was demonstrated that the resolution of the characteristic-wise WENO schemes is superior to that of their component-wise counterpart. Most notably, solutions are much less oscillatory.

In a later paper [16], Donat and Mulet showed that the hyperbolicity calculus of multi-species kinematic flow models can be greatly simplified if one employs the so-called secular equation due to Anderson [1]. Roughly speaking, the secular equation provides a systematic algebraic framework to determine the eigenvalues, and eventually the eigenvectors if the Jacobian is a rank-m, $m \ll N$, perturbation of the diagonal, and most importantly avoids the explicit representation of the characteristic polynomial. Donat and Mulet [16] showed that via the secular approach, hyperbolicity of the MLB model for equal-density spheres (a case of $m = 2$) can be proved in a few lines, which contrasts with several pages of computation necessary to exhibit the characteristic polynomial in [7]. In [9] we showed that the secular approach can also be used to estimate the region of hyperbolicity of the HS model, which corresponds to $m = 3$ or $m = 4$. In this paper, we use the results of [9] to provide a counterpart of [17] for the MLB and HS models, namely we show that the results in [9] permit to implement characteristic-wise WENO schemes, and that these are robust and have favorable properties analogous to those in [17].

1.3. **Outline of the paper.** The remainder of the paper is organized as follows. In Sections 2.1 and 2.2 the MLB and HS models are recalled. The relevant parts of the hyperbolicity analysis of [9, 16], which permits to extract the relevant spectral information for the implementation of WENO schemes, are summarized in Section 2.4. The numerical schemes are described in Section 3, starting with a spatially semi-discrete formulation and the implementation of the boundary conditions (Sects. 3.1 and 3.2), which is converted into a fully discrete scheme by a strong stability preserving Runge-Kutta scheme (SSPRK; Sect. 3.3). We then proceed with a general discussion of flux vector splitting (Sect. 3.4). Then, in Sections 3.4, and 3.5, which are at the core of this paper, we describe how the explicit algebraic form of the velocities $v_1, \dots, v_N$ in conjunction with the characteristic information, namely the interlacing property of eigenvalues with phase velocities and the left eigenvectors, can be used to define viscosity coefficients for the characteristic-wise computation of the flux vectors. The resulting scheme is addressed by SPEC-INT scheme; its counterpart based on less involved component-wise flux vector splitting is referred to as COMP-GLF scheme. In Section 4 we present a series of numerical examples for the MLB model with $N = 2$, 4 and 11, along with error histories, that illustrate the superiority of SPEC-INT (compared with COMP-GLF) in terms of accuracy. Additional examples suggest that the scheme is equally suitable for the HS model. Finally, in Section 5 we list some conclusions, address limitations of the applicability of the scheme and point out possible extensions.

2. The polydisperse sedimentation models

2.1. **The MLB model.** The Masliyah-Lockett-Bassoon (MLB) model arises from the continuity and linear momentum balance equations for the solid species and the fluid. Its detailed derivation is presented e.g. in [7, 12], so we will introduce the model here in its final form. For particles that have the same density, the velocities $v_1(\Phi), \dots, v_N(\Phi)$ are given by

$$v_i(\Phi) = \frac{(\varrho_\mathrm{s} - \varrho_\mathrm{f})gD_1^2}{18\mu_\mathrm{f}}(1-\phi)\Big(d_i^2 V_i(\phi) - \big(\phi_1 d_1^2 V_1(\phi) + \cdots + \phi_N d_N^2 V_N(\phi)\big)\Big), \quad i = 1, \dots, N, \tag{2.1}$$

where ϱ_s and ϱ_f are the solid and fluid densities, g is the acceleration of gravity, μ_f is the fluid viscosity, $\phi = \phi_1 + \cdots + \phi_N$ is the total solids volume fraction, and $V_1, \dots, V_N$ are hindered settling factors that are in general particle-size-specific [2]. In this work, we limit ourselves to the case (originally proposed in [29, 30]) of a collective hindered settling factor $V(\phi) := V_1(\phi) = \cdots = V_N(\phi)$, for which (2.1) can be written as

$$v_i(\Phi) = v_i^{\mathrm{MLB}}(\Phi) := \frac{(\varrho_\mathrm{s} - \varrho_\mathrm{f})gD_1^2}{18\mu_\mathrm{f}}(1-\phi)V(\phi)\big(d_i^2 - (\phi_1 d_1^2 + \cdots + \phi_N d_N^2)\big), \quad i = 1, \dots, N, \tag{2.2}$$

and where $V(\phi)$ is assumed to satisfy

$$V(0) = 1, \quad V(\phi_{\max}) = 0, \quad V'(\phi) \le 0 \quad \text{for } \phi \in [0, \phi_{\max}], \tag{2.3}$$

where the maximum total solids concentration is assumed to be given by the constant $\phi_{\max}$. A standard choice for $V(\phi)$ is the equation

$$V(\phi) = \begin{cases} (1-\phi)^{n-2} & \text{if } \Phi \in \mathcal{D}_{\phi_{\max}} \\ 0 & \text{otherwise,} \end{cases} \qquad n > 2. \tag{2.4}$$

We may write the components $f_i(\Phi)$, $i = 1, \dots, N$ of the flux vector $\mathbf{f}(\Phi)$ of the MLB model as

$$f_i(\Phi) = f_i^{\mathrm{MLB}}(\Phi) := v_1^{\mathrm{MLB}}(\mathbf{0})\phi_i(1-\phi)V(\phi)\big(d_i^2 - (\phi_1 d_1^2 + \cdots + \phi_N d_N^2)\big), \quad i = 1, \dots, N. \tag{2.5}$$

2.2. **HS model.** The Höfler and Schwarzer (HS) model is motivated by a formula by Batchelor [3] and Batchelor and Wen [4], who advanced the following expression for v_i for a dilute suspension (i.e., $\phi \ll \phi_{\max}$):

$$v_i(\Phi) = \frac{(\varrho_\mathrm{s} - \varrho_\mathrm{f})gD_1^2}{18\mu_\mathrm{f}} d_i^2 (1 + \mathbf{s}_i^{\mathrm{T}}\Phi), \quad i = 1, \dots, N. \tag{2.6}$$

Here, $\mathbf{s}_i^{\mathrm{T}} := (S_{i1}, \dots, S_{iN})$ is the i-th row of the matrix $\mathbf{S} = (S_{ij})_{1\le i,j\le N}$ of dimensionless sedimentation coefficients S_{ij}, which are negative functions of $\lambda_{ij} := d_j/d_i$ and depend on certain other parameters, see [3, 4] for details. The coefficients S_{ij} can be reasonably approximated by the formula

$$S_{ij} = \sum_{l=0}^{3} \beta_l \left(\frac{d_j}{d_i}\right)^l, \quad 1 \le i,j \le N \quad \text{with coefficients } \beta_0, \dots, \beta_3 \le 0. \tag{2.7}$$

Davis and Gecol [14] employed (2.7) to approximate the numerical values of S_{ij} tabulated in [4] for eight different values of λ_{ij}. They obtained $\beta_i < 0$ for $i = 0, \dots, 3$, with small values of $|\beta_3|$. In light of a theoretical asymptotical result [3], some authors set $\beta_3 = 0$ a priori; for example, Höfler and Schwarzer [24] obtained

$$\boldsymbol{\beta}^{\mathrm{T}} = (\beta_0, \dots, \beta_3) = (-3.52, -1.04, -1.03, 0) \tag{2.8}$$

by fitting data from [4] to a second-order polynomial. For simplicity, we consider $\beta_3 = 0$ also in this work.

To overcome the limitation of (2.6) to dilute suspensions, formal extensions of (2.6) to the whole range of concentrations have been proposed. In particular, Höfler and Schwarzer [10, 23, 24] advanced the equation

$$v_i(\Phi) = v_i^{\mathrm{HS}}(\Phi) := \frac{(\varrho_{\mathrm{s}} - \varrho_{\mathrm{f}})gD_1^2}{18\mu_{\mathrm{f}}} d_i^2 \exp(\mathbf{s}_i^{\mathrm{T}}\Phi + n\phi)(1-\phi)^n, \quad n \ge 0. \tag{2.9}$$

For $\Phi \to 0$, (2.9) has the same partial derivatives as (2.6), while for $\phi \to 1$, the velocities v_i given by (2.9) vanish. The corresponding flux vector of the HS model is given by

$$f_i(\Phi) = f_i^{\mathrm{HS}}(\Phi) := v_1^{\mathrm{HS}}(\mathbf{0})\phi_i d_i^2 \exp(\mathbf{s}_i^{\mathrm{T}}\Phi + n\phi)(1-\phi)^n, \quad i = 1, \dots, N. \tag{2.10}$$

For the HS model it is straightforward to verify strict hyperbolicity on $\mathcal{D}_1$ for $N = 2$, arbitrary non-positive Batchelor matrices $\mathbf{S}$ and arbitrarily small values of d_2. The analysis of [9] ensures hyperbolicity for arbitrary N and in the case of the coefficients (2.8) under the fairly mild restriction $d_N > 0.0078595$. These properties contrast with those of the model by Davis and Gecol [14], which equally extends (2.6) to the full range of concentration vectors but is strictly hyperbolic under very restrictive conditions only [12].

2.3. **A variant of the HS model.** In order to ensure that $v_i \to 0$ continuously for the HS model when $\phi \to \phi_{\max}$ we consider the following variant (see [24]) of the HS model:

$$v_i(\Phi) = v_1^{\mathrm{HS}}(\mathbf{0}) d_i^2 \exp\left(\mathbf{s}_i^{\mathrm{T}}\Phi + n\frac{\phi}{\phi_{\max}}\right)\left(1 - \frac{\phi}{\phi_{\max}}\right)^n, \quad n \ge 0, \tag{2.11}$$

which is defined for $\Phi \in \mathcal{D}_{\phi_{\max}}$. As we will see, the results of the available hyperbolicity analysis for the HS model in Section 2.2, which consists in setting $\phi_{\max} = 1$ in (2.11) but cutting the domain where (2.9) is valid abruptly at the boundary of $\mathcal{D}_{\phi_{\max}}$, can be readily employed to analyze the hyperbolicity of the model given by (2.11), to which we will refer as the "modified HS model".

2.4. **Hyperbolicity analysis.** For the MLB and HS models, the velocities $v_1, \dots, v_N$ do not depend on each of the N components of Φ in an individual way, but are functions of a small number $m \ll N$ of scalar functions of Φ, i.e.,

$$v_i = v_i(p_1, \dots, p_m), \quad p_l = p_l(\Phi), \quad i = 1, \dots, N, \quad l = 1, \dots, m. \tag{2.12}$$

This means that for both models, the entries $f_{ij}(\Phi) := \partial f_i(\Phi)/\partial\phi_j$ of the Jacobian $\mathcal{J}_{\mathbf{f}}(\Phi)$ are given by

$$f_{ij} = \frac{\partial(\phi_i v_i)}{\partial \phi_j} = v_i\delta_{ij} + \sum_{l=1}^{m} \phi_i \frac{\partial v_i}{\partial p_l}\frac{\partial p_l}{\partial \phi_j}, \quad i,j = 1, \dots, N, \tag{2.13}$$

i.e., $\mathcal{J}_{\mathbf{f}}(\Phi)$ is a rank-m perturbation of the diagonal matrix $\mathbf{D} := \mathrm{diag}(v_1, \dots, v_N)$ of the form

$$\mathcal{J}_{\mathbf{f}} = \mathbf{D} + \mathbf{B}\mathbf{A}^{\mathrm{T}}, \quad \begin{cases} \mathbf{B} := (B_{il}) = (\phi_i \partial v_i/\partial p_l), \\ \mathbf{A} := (A_{jl}) = (\partial p_l/\partial \phi_j), \end{cases} \quad 1 \le i,j \le N, \quad 1 \le l \le m. \tag{2.14}$$

The hyperbolicity analysis is then based on the following theorem, which can be found in [1], but we give here the form in [16], which provides the explicit formulas to be used in the applications.

Theorem 2.1 (The secular equation, [1, 16]). *Assume that $v_i > v_j$ for $i < j$, and that $\mathbf{A}$ and $\mathbf{B}$ have the formats specified in* (2.14). *We denote by S_r^p the set of all (ordered) subsets of r elements taken from a set of p elements. If $\mathbf{X}$ is an $m \times N$ matrix, $I := \{i_1 < \ldots < i_k\} \in S_k^N$ and $J := \{j_1 < \ldots < j_l\} \in S_l^m$, then we denote by $\mathbf{X}^{I,J}$ the $k \times l$ submatrix of $\mathbf{X}$ given by $(\mathbf{X}^{I,J})_{p,q} = X_{i_p,j_q}$. Let $\lambda \neq v_i$ for $i = 1, \ldots, N$. Then λ is an eigenvalue of $\mathbf{D} + \mathbf{B}\mathbf{A}^{\mathrm{T}}$ if and only if*

$$R(\lambda) := \det\left[\mathbf{I} + \mathbf{A}^{\mathrm{T}}(\mathbf{D} - \lambda\mathbf{I})^{-1}\mathbf{B}\right] = 1 + \sum_{i=1}^{N} \frac{\gamma_i}{v_i - \lambda} = 0. \tag{2.15}$$

The coefficients γ_i, $i = 1, \ldots, N$, are given by the following expression:

$$\gamma_i = \sum_{r=1}^{\min\{N,m\}} \sum_{i \in I \in S_r^N, J \in S_r^m} \frac{\det \mathbf{A}^{I,J} \det \mathbf{B}^{I,J}}{\prod_{l \in I, l \neq i}(v_l - v_i)}. \tag{2.16}$$

The relation $R(\lambda) = 0$ is known as the secular equation [1].

Assuming that $m < N$, with $\mathbf{A}$ and $\mathbf{B}$ defined in (2.14) we can write

$$\det \mathbf{A}^{I,J} = \det\left(\frac{\partial p_J}{\partial \phi_I}\right), \quad \det \mathbf{B}^{I,J} = \det\left(\frac{\partial v_I}{\partial p_J}\right) \prod_{l \in I} \phi_l,$$

where the notation above should be self-explanatory. Then, we can write

$$\gamma_i = \phi_i \sum_{r=1}^{m} \gamma_{r,i}, \quad \gamma_{r,i} = \sum_{i \in I \in S_r^N} \prod_{l \in I, l \neq i} \frac{\phi_l}{v_l - v_i} \sum_{J \in S_r^m} \det\left(\frac{\partial v_I}{\partial p_J}\right) \det\left(\frac{\partial p_J}{\partial \phi_I}\right). \tag{2.17}$$

When $m \leq 2$, these quantities can be easily computed and the hyperbolicity analysis via the secular equation is much less involved than explicitly deriving $\det(\mathcal{J}_{\mathbf{f}}(\Phi) - \lambda\mathbf{I})$, and discussing its zeros, as was done in [7, 33]. For $m = 3$ or $m = 4$, the computations in the secular equation performed in [9] are more involved, but have turned out very useful in providing at least partial results concerning hyperbolicity, where the theoretical analysis of $\det(\mathcal{J}_{\mathbf{f}}(\Phi) - \lambda\mathbf{I})$ is essentially out of reach.

The following corollary illustrates the importance of the secular equation. Its proof (see [9]) follows from Theorem 2.1 by a discussion of the poles of $R(\lambda)$ and its asymptotic behaviour as $\lambda \to \pm\infty$.

Corollary 2.1 ([9]). *With the notation of Theorem 2.1, assume that $\gamma_i \cdot \gamma_j > 0$ for $i, j = 1, \ldots, N$. Then $\mathbf{D} + \mathbf{B}\mathbf{A}^{\mathrm{T}}$ is diagonalizable with real eigenvalues $\lambda_1, \ldots, \lambda_N$. If $\gamma_1, \ldots, \gamma_N < 0$, the* interlacing property

$$M_1 := v_N + \gamma_1 + \cdots + \gamma_N < \lambda_N < v_N < \lambda_{N-1} < \ldots < \lambda_1 < v_1 \tag{2.18}$$

holds, while for $\gamma_1, \ldots, \gamma_N > 0$, the following analogous property holds:

$$v_N < \lambda_N < v_{N-1} < \lambda_{N-1} < \ldots < v_1 < \lambda_1 < M_2 := v_1 + \gamma_1 + \cdots + \gamma_N. \tag{2.19}$$

The analysis of [9] related to the secular equation also permits to obtain an explicit expression of the spectral decomposition of $\mathcal{J}_{\mathbf{f}} = \mathcal{J}_{\mathbf{f}}(\Phi)$ needed for the implementation of spectral schemes. Assume λ is an eigenvalue of $\mathcal{J}_{\mathbf{f}}$ that satisfies $\lambda \neq v_i$ for all $i = 1, \ldots, N$. Then $\boldsymbol{\xi} = \mathbf{A}^{\mathrm{T}}\mathbf{x}$ is a solution of $\mathbf{M}_\lambda \boldsymbol{\xi} = \mathbf{0}$, where the $m \times m$ matrix $\mathbf{M}_\lambda := \mathbf{I} + \mathbf{A}^{\mathrm{T}}(\mathbf{D} - \lambda\mathbf{I})^{-1}\mathbf{B}$ can easily be computed. In fact, given two vectors $\mathbf{g} = (g_1, \ldots, g_N)^{\mathrm{T}}, \mathbf{h} = (h_1, \ldots, h_N)^{\mathrm{T}} \in \mathbb{R}^N$, if we use the notation

$$[\mathbf{g}, \mathbf{h}] := [\mathbf{g}, \mathbf{h}]_\lambda := \mathbf{g}^{\mathrm{T}}(\mathbf{D} - \lambda\mathbf{I})^{-1}\mathbf{h} = \sum_{k=1}^{N} \frac{g_k h_k}{v_k - \lambda} \tag{2.20}$$

and denote by $\mathbf{a}_i$ and $\mathbf{b}_j$ the columns of $\mathbf{A}$ and $\mathbf{B}$, respectively, then $\mathbf{M}_\lambda = \mathbf{I} + ([\mathbf{a}_i, \mathbf{b}_j])_{1 \leq i,j \leq m}$. Provided that we can compute a solution $\boldsymbol{\xi} \neq \mathbf{0}$ of $\mathbf{M}_\lambda \boldsymbol{\xi} = \mathbf{0}$, we can use the relation $\mathbf{x} + (\mathbf{D} - \lambda\mathbf{I})^{-1}\mathbf{B}(\mathbf{A}^{\mathrm{T}}\mathbf{x}) = \mathbf{0}$ to compute a right eigenvector of $\mathcal{J}_{\mathbf{f}}$ as

$$\mathbf{x} = -(\mathbf{D} - \lambda\mathbf{I})^{-1}\mathbf{B}\boldsymbol{\xi}. \tag{2.21}$$

The same procedure may be employed to calculate the left eigenvectors of $\mathcal{J}_{\mathbf{f}}$, since they are the right eigenvectors of $\mathcal{J}_{\mathbf{f}}^{\mathrm{T}} = \mathbf{D} + \mathbf{A}\mathbf{B}^{\mathrm{T}}$, so the roles of $\mathbf{A}$ and $\mathbf{B}$ and corresponding columns just need to be interchanged.

The version of the MLB model introduced in Section 2.1 corresponds to $m = 2$, where one may choose $p_1 = \phi$ and $p_2 = V(\phi)(d_1^2\phi_1 + \cdots + d_N^2\phi_N)$. For this model, the following lemma is proved in [9] as a consequence of Corollary 2.1 and the discussion of the computation of left and right eigenvectors.

Lemma 2.1. *The MLB model for equal-density spheres* (1.1), (2.5) *is strictly hyperbolic for all* $\Phi \in \mathcal{D}_{\phi_{\max}}$. *The eigenvalues* $\lambda_i = \lambda_i(\Phi)$ *of the Jacobian* $\mathcal{J}_{\mathbf{f}}(\Phi) = \mathcal{J}_{\mathbf{f}^{\mathrm{MLB}}}(\Phi)$ *satisfy the interlacing property*

$$M_1(\Phi) < \lambda_N(\Phi) < v_N(\Phi) < \lambda_{N-1}(\Phi) < v_{N-1}(\Phi) < \ldots < \lambda_1(\Phi) < v_1(\Phi) \tag{2.22}$$

where the lower bound is given by

$$M_1(\Phi) := v_N(\Phi) + \sum_{k=1}^{N} \gamma_k = v_1^{\mathrm{MLB}}(\mathbf{0})\Big(d_N^2 V(\Phi) + \big((1-\phi)V'(\phi) - 2V(\phi)\big)(d_1^2\phi_1 + \cdots + d_N^2\phi_N)\Big).$$

The right and left eigenvectors of $\mathcal{J}_{\mathbf{f}}(\Phi)$, *denoted by* $\mathbf{x} = (x_1, \ldots, x_N)^{\mathrm{T}}$ *and* $\mathbf{y} = (y_1, \ldots, y_N)^{\mathrm{T}}$, *respectively, that correspond to a root* λ *of the secular equation are*

$$x_i = \frac{1}{v_i - \lambda}\left[b_{i,1}\sum_{k=1}^{N}\frac{a_{k,1}b_{k,2}}{v_k - \lambda} - b_{i,2}\left(1 + \sum_{k=1}^{N}\frac{a_{k,1}b_{k,1}}{v_k - \lambda}\right)\right], \quad i = 1, \ldots, N, \tag{2.23}$$

$$y_i = \frac{1}{v_i - \lambda}\left[a_{i,1}\sum_{k=1}^{N}\frac{b_{k,1}a_{k,2}}{v_k - \lambda} - a_{i,2}\left(1 + \sum_{k=1}^{N}\frac{b_{k,1}a_{k,1}}{v_k - \lambda}\right)\right], \quad i = 1, \ldots, N, \tag{2.24}$$

where

$$b_{i,1} = \phi_i d_i^2 V'(\phi), \quad b_{i,2} = -\phi_i, \quad a_{i,1} = 1, \quad a_{i,2} = V'(\phi)(d_1^2\phi_1 + \cdots + d_N^2\phi_N) + d_i^2 V(\phi). \tag{2.25}$$

For the HS model, we define

$$\mathbf{a}_\nu := \mathbf{d}_{\nu-1}^{\mathrm{T}} := (d_1^{\nu-1}, d_2^{\nu-1}, \ldots, d_N^{\nu-1}), \quad p_\nu := \mathbf{a}_\nu^{\mathrm{T}}\Phi, \quad \nu = 1, \ldots, 4, \tag{2.26}$$

and taking into account that $\beta_3 = 0$, we write

$$\mathbf{s}_i^{\mathrm{T}}\Phi = \sum_{j=1}^{N}\left(\sum_{\nu=0}^{2}\beta_\nu\left(\frac{d_j}{d_i}\right)^\nu\right)\phi_j = \sum_{\nu=0}^{2}\frac{\beta_\nu}{d_i^\nu}\mathbf{a}_\nu^{\mathrm{T}}\Phi = \sum_{\nu=0}^{2}\frac{\beta_\nu}{d_i^\nu}p_{\nu+1}, \quad i = 1, \ldots, N.$$

We may then express (2.9) as

$$v_i(\Phi) = v_i(p_1, \ldots, p_3) = v_1^{\mathrm{HS}}(\mathbf{0})d_i^2\exp\big((\beta_0 + n)p_1 + \beta_1 d_i^{-1}p_2 + \beta_2 d_i^{-2}p_3\big)(1 - p_1)^n, \quad i = 1, \ldots, N. \tag{2.27}$$

The entries of the matrices $\mathbf{A}$ and $\mathbf{B}$, namely $a_i^k = \partial p_k/\partial\phi_i$ and $b_i^k = \phi_i\partial v_i/\partial p_k$, are now given by

$$a_i^k = d_i^{k-1}, \quad b_i^k = d_i^{3-k}\phi_i(1 - p_1)^n\tilde{\beta}_{k-1}\exp(\mathbf{s}_i^{\mathrm{T}}\Phi + n\phi), \quad \tilde{\beta}_0 = \beta_0 - \frac{np_1}{1 - p_1}, \quad \tilde{\beta}_k = \beta_k, \quad k = 1, 2.$$

The hyperbolicity analysis of the HS model carried out in [9] is considerably more involved than that of the MLB model. The following lemma summarizes the results obtained in [9] for the HS model.

Lemma 2.2. *Assume that the vector of parameters* $\boldsymbol{\beta}$, *the maximum solids concentration* $\phi_{\max}$ *and the width of the particle size distribution, characterized by the value of* $d_N \in (0, 1]$, *satisfy the inequality*

$$H(\phi, \boldsymbol{\beta}, d_N) := -\tilde{\beta}_0\big(\beta_1 d_N + \beta_2(1 + d_N)^2\big) - \beta_2\beta_1 d_N - \phi(1 - d_N)^2\tilde{\beta}_0\beta_1\beta_2 < 0. \tag{2.28}$$

Then the HS model is strictly hyperbolic for $\Phi \in \mathcal{D}_{\phi_{\max}}$. *Furthermore, the eigenvalues satisfy the interlacing property (2.22), with* $M_1(\Phi) := v_N(\Phi) + \sum_{k=1}^{N}\gamma_k$ *and*

$$\gamma_i = v_1^{\mathrm{HS}}(\mathbf{0})\phi_i(1 - \phi)^n\exp(\mathbf{s}_i^{\mathrm{T}}\Phi + n\phi)\left(\mathcal{S}_{1,i} + \mathcal{S}_{2,i} + \mathcal{S}_{3,i}\right), \tag{2.29}$$

where in terms of $\tilde{\eta}_i := \exp(\mathbf{s}_i^{\mathrm{T}}\Phi)$ *we define*

$$\mathcal{S}_{1,i} := d_i^2\big(\tilde{\beta}_0 + \beta_1 + \beta_2\big),$$

$$\mathcal{S}_{2,i} := -\sum_{\substack{j=1\\ j\neq i}}^{N} \frac{\phi_j\tilde{\eta}_j}{d_j^2\tilde{\eta}_j - d_i^2\tilde{\eta}_i}\Big\{(d_i-d_j)^2\tilde{\beta}_0\big(\beta_1 d_i d_j + \beta_2(d_i+d_j)^2\big) + \beta_1\beta_2 d_i d_j (d_i-d_j)^2\Big\},$$

$$\mathcal{S}_{3,i} := -\tilde{\beta}_0\beta_1\beta_2 \sum_{\substack{j,k=1\\ j<k,\, j,k\neq i}}^{N} \frac{\phi_j\phi_k\tilde{\eta}_j\tilde{\eta}_k\pi_{ijk}^2}{(d_k^2\tilde{\eta}_k - d_i^2\tilde{\eta}_i)(d_j^2\tilde{\eta}_j - d_i^2\tilde{\eta}_i)}, \quad \pi_{ijk} := (d_j-d_i)(d_k-d_i)(d_k-d_j).$$

The spectral decomposition of $\mathcal{J}_{\mathbf{f}}(\Phi)$ is not provided in [9] in a form similar to that in Lemma 2.1, but it is easy to obtain from Theorem 2.1. According to Theorem 2.1, if $\lambda \neq v_i$ is an eigenvalue of $\mathcal{J}_{\mathbf{f}}(\Phi)$, then $\det \mathbf{M}_\lambda = 0$ and therefore $\boldsymbol{\xi} = (\xi_1,\xi_2,\xi_3)$ is a non-trivial solution of $\mathbf{M}_\lambda\boldsymbol{\xi} = \mathbf{0}$ for

$$\begin{aligned}
\xi_1 &= (1+[\mathbf{a}_2,\mathbf{b}_2])(1+[\mathbf{a}_3,\mathbf{b}_3]) - [\mathbf{a}_2,\mathbf{b}_3][\mathbf{a}_3,\mathbf{b}_2],\\
\xi_2 &= [\mathbf{a}_2,\mathbf{b}_3][\mathbf{a}_3,\mathbf{b}_1] - [\mathbf{a}_2,\mathbf{b}_1](1+[\mathbf{a}_3,\mathbf{b}_3]),\\
\xi_3 &= [\mathbf{a}_2,\mathbf{b}_1][\mathbf{a}_3,\mathbf{b}_2] - (1+[\mathbf{a}_2,\mathbf{b}_2])[\mathbf{a}_3,\mathbf{b}_1].
\end{aligned}$$

Hence, by using (2.21) we obtain the following right eigenvector $\mathbf{x} = (x_1,\ldots,x_N)^{\mathrm{T}}$ for the HS model:

$$x_i = -\frac{1}{v_i-\lambda}\left(b_{i,1}\xi_1 + b_{i,2}\xi_2 + b_{i,3}\xi_3\right), \quad i = 1,\ldots,N. \tag{2.30}$$

The left eigenvectors can be obtained by interchanging the roles of $\mathbf{A}$ and $\mathbf{B}$.

Finally, let us come back to the modified HS model (2.11) considered in this paper. Introducing the variable $\hat{\Phi} := (\phi_{\max}^{-1})\Phi$ we can write (2.11) as follows:

$$v_i(\hat{\Phi}) = v_1^{\mathrm{HS}}(\mathbf{0})d_i^2\exp\big(\hat{\mathbf{s}}_i^{\mathrm{T}}\hat{\Phi} + n\hat{\phi}\big)\big(1-\hat{\phi}\big)^n = v_1^{\mathrm{HS}}(\mathbf{0})d_i^2\exp\big((\hat{\beta}_0+n)\hat{p}_1 + \hat{\beta}_1 d_i^{-1}\hat{p}_2 + \hat{\beta}_2 d_i^{-2}\hat{p}_3\big)(1-\hat{p}_1)^n$$

where $\hat{\mathbf{s}}_i^{\mathrm{T}} = (\hat{S}_{i1},\ldots,\hat{S}_{iN})^{\mathrm{T}} = \phi_{\max}\mathbf{s}_i^{\mathrm{T}}$, $i = 1,\ldots,N$. The available hyperbolicity analysis for the HS model can be applied to analyze the hyperbolicity of the modified HS model if we define the coefficients $\hat{\beta}_k := \phi_{\max}\beta_k$ for $k = 0,1,2$ and the quantities $\hat{p}_\nu = \mathbf{a}_\nu^{\mathrm{T}}\hat{\Phi}$, $\nu = 1,2,3$. We can now apply Lemma 2.2 to deduce that the modified HS model is strictly hyperbolic if

$$H(\hat{\phi},\hat{\boldsymbol{\beta}},d_N) := -\tilde{\hat{\beta}}_0\big(\hat{\beta}_1 d_N + \hat{\beta}_2(1+d_N)^2\big) - \hat{\beta}_2\hat{\beta}_1 d_N - \hat{\phi}(1-d_N)^2\tilde{\hat{\beta}}_0\hat{\beta}_1\hat{\beta}_2 < 0, \tag{2.31}$$

where we define

$$\tilde{\hat{\beta}}_0 = \hat{\beta}_0 - \frac{n\hat{\phi}}{1-\hat{\phi}}.$$

Assume now that the original coefficients $\boldsymbol{\beta}$ are given by (2.8). Then a simple algebraic computation shows that (2.31) holds if $d_N > 0.0078595$, that is, with the same mild restriction of the original HS model. This is the matter of the next lemma.

Lemma 2.3. *Assume that the coefficients $\boldsymbol{\beta}$ are given by* (2.8)*. Then the modified HS model specified by phase velocities v_i given by* (2.11) *is strictly hyperbolic on $\mathcal{D}_{\phi_{\max}}$ if $d_N > 0.0078595$.*

Proof. To make the basic idea transparent, let us write $\hat{\phi}(\phi) = \phi/\phi_{\max}$ and $\hat{\boldsymbol{\beta}}(\boldsymbol{\beta}) = \phi_{\max}\boldsymbol{\beta}$. Then it is sufficient to notice that we can write

$$H\big(\hat{\phi}(\phi),\hat{\boldsymbol{\beta}}(\boldsymbol{\beta}),d_N\big) = \phi_{\max}^2\big(H(\phi,\boldsymbol{\beta},d_N) - C\widetilde{H}(\phi,\boldsymbol{\beta},d_N)\big), \tag{2.32}$$

where

$$\widetilde{H}(\phi,\boldsymbol{\beta},d_N) := \big(\beta_1 d_N + \beta_2(1+d_N)^2 + \phi(1-d_N)^2\beta_1\beta_2\big), \quad C := n\phi\left(\frac{1}{1-\phi} - \frac{1}{\phi_{\max}(\phi_{\max}-\phi)}\right) < 0.$$

Since the variant of the model is strictly hyperbolic if $H(\hat{\phi}(\phi),\hat{\boldsymbol{\beta}}(\boldsymbol{\beta}),d_N) < 0$, it is sufficient to show that $\widetilde{H}(\phi,\boldsymbol{\beta},d_N) < 0$, but this statement is true if $d_N > 0.0078595$. □

3. Numerical schemes

3.1. **Semi-discrete schemes.** The schemes considered herein are based on the finite difference paradigm due to Shu and Osher [38] of first setting up a conservative spatial semi-discretization of the term $\partial_x \mathbf{f}(\Phi)$ and then to apply an SSP ODE solver to get a fully discrete conservative scheme with a high order of accuracy. Specifically, if we discretize the spatial domain $[0,1]$ (after normalization) into M cells of size $\Delta x = 1/M$ and define the cell centers $x_j := (j+1/2)\Delta x$, $j = 0, \dots, M-1$ and the cell interfaces $x_{j+1/2} = (j+1)\Delta x$, then the approximation to $\partial_x \mathbf{f}(x_j, t)$ is obtained by an essentially non-oscillatory reconstruction operator, $\boldsymbol{\mathcal{R}}$, applied to the fluxes $\mathbf{f}(\Phi)$ so that:

$$\partial_x \mathbf{f}(x_j, t) = \frac{1}{\Delta x}\left(\hat{\mathbf{f}}_{j+1/2} - \hat{\mathbf{f}}_{j-1/2}\right) + \mathcal{O}(\Delta x^r),$$

where r is the order of accuracy of the reconstruction and the numerical fluxes $\hat{\mathbf{f}}_{j+1/2}$ are given by

$$\hat{\mathbf{f}}_{j+1/2} = \boldsymbol{\mathcal{R}}\Big(\mathbf{f}\big(\Phi(x_{j-s}, t)\big), \dots, \mathbf{f}\big(\Phi(x_{j+s+1}, t)\big); x_{j+1/2}\Big) = \hat{\mathbf{f}}_{j+1/2}\big(\Phi(x_{j-s}, t), \dots, \Phi(x_{j+s+1}, t)\big). \tag{3.1}$$

If we define the vector $\boldsymbol{\Phi} := (\Phi_{-s}, \Phi_{-s+1}, \dots, \Phi_{M+s-2}, \Phi_{M+s-1})^{\mathrm{T}}$, this procedure yields the semi-discrete scheme (method of lines)

$$\frac{\mathrm{d}\Phi_j}{\mathrm{d}t} = \mathcal{L}_j(\boldsymbol{\Phi}) := -\frac{1}{\Delta x}\big(\hat{\mathbf{f}}_{j+1/2}(\Phi_{j-s}, \dots, \Phi_{j+s+1}) - \hat{\mathbf{f}}_{j-1/2}(\Phi_{j-s-1}, \dots, \Phi_{j+s})\big), \quad j = 0, \dots, M-1. \tag{3.2}$$

for approximations $\Phi_j(t) \approx \Phi(x_j, t)$, $j = 0, \dots, M-1$. If we define the vector $\boldsymbol{\mathcal{L}} := (\mathcal{L}_0, \dots, \mathcal{L}_{M-1})^{\mathrm{T}}$, then (3.2) can be compactly written as

$$\frac{\mathrm{d}\boldsymbol{\Phi}(t)}{\mathrm{d}t} = \boldsymbol{\mathcal{L}}\big(\boldsymbol{\Phi}(t)\big). \tag{3.3}$$

For well-known stability reasons, the reconstruction operator should be "upwind-biased". In the scalar case, this means that $\mathcal{R}$ should not depend on its last argument if $f' > 0$ and should not depend on its first argument if $f' < 0$. For nonlinear fluxes (mandatorily near sonic points, where $f' = 0$) a flux splitting approach, where

$$f = f^- + f^+, \quad f_u^+ > 0, \quad f_u^- < 0,$$

is used in order to define the numerical flux, so that

$$\hat{f}_{j+1/2} = \mathcal{R}^+\big(f^+(\Phi_{j-s}), \dots, f^+(\Phi_{j+s}); x_{j+1/2}\big) + \mathcal{R}^-\big(f^-(\Phi_{j-s+1}), \dots, f^-(\Phi_{j+s+1}); x_{j+1/2}\big), \tag{3.4}$$

for upwind-biased reconstructions $\mathcal{R}^{\pm}$. In this work, $\mathcal{R}^{\pm}$ is chosen as the mapped WENO5 (WENO5M) reconstruction, proposed in [26], to avoid a possible loss of accuracy around extrema. This technique can be extended to vectors of fluxes by its application either to each component of the system ("component-wise" schemes) or by local characteristic projections ("characteristic-wise" schemes).

3.2. **Boundary conditions.** The zero-flux boundary conditions (1.3) are implemented by setting

$$\hat{\mathbf{f}}_{-1/2} = \hat{\mathbf{f}}_{M-1/2} = 0. \tag{3.5}$$

We recall that a WENO5 scheme requires to consider two additional ghost cells on each boundary of the computational domain. In order to guarantee that all the interpolatory stencils remain inside of the computational domain we employ a suggestion given in [39]: we set large values for the concentrations in the ghost cells, which produce large variations, so that the WENO procedure avoids the use of any stencil involving the ghost cells.

3.3. **Time discretization.** Among the variety of explicit SSP (*strong-stability preserving*) time discretization methods for the approximate solution of (3.3) we use the well known optimal third-order, three-stage Runge-Kutta method referred to as SSPRK(3,3), which for (3.3) is given by

$$\begin{aligned}\boldsymbol{\Phi}^{(1)} &= \boldsymbol{\Phi}^{\nu} + \Delta t \boldsymbol{\mathcal{L}}\big(\boldsymbol{\Phi}^{\nu}\big),\\ \boldsymbol{\Phi}^{(2)} &= \frac{3}{4}\boldsymbol{\Phi}^{\nu} + \frac{1}{4}\boldsymbol{\Phi}^{(1)} + \frac{1}{4}\Delta t \boldsymbol{\mathcal{L}}\big(\boldsymbol{\Phi}^{(1)}\big),\\ \boldsymbol{\Phi}^{\nu+1} &= \frac{1}{3}\boldsymbol{\Phi}^{\nu} + \frac{2}{3}\boldsymbol{\Phi}^{(2)} + \frac{2}{3}\Delta t \boldsymbol{\mathcal{L}}\big(\boldsymbol{\Phi}^{(2)}\big).\end{aligned} \tag{3.6}$$

SSP time discretization methods are widely used for hyperbolic PDE because they preserve the nonlinear stability properties which are necessary for problems with non-smooth solutions. On the other hand, due to convexity, the intermediate stages of the SSPRK methods have SSP properties (*i.e.*, $\|\boldsymbol{\Phi}^{(i)}\| \leq \|\boldsymbol{\Phi}^{(i-1)}\|$ for the internal stages). This feature is especially important for some applications [19]. For sedimentation problems it avoids unphysical negative concentrations in the internal stages. Notice that it is necessary to evaluate three times the operator $\boldsymbol{\mathcal{L}}(\cdot)$ in order to move forward one time step, in fact, the *effective SSP coefficient* for SSPRK(3,3) (which is defined as [19, 34, 35] the SSP coefficient of the method divided by the number of stages) is equal to 1/3.

To satisfy the CFL condition the value of Δt is computed adaptively for each step ν. More exactly, the solution $\boldsymbol{\Phi}^{\nu+1}$ at $t_{\nu+1} = t_{\nu} + \Delta t$ is calculated from $\boldsymbol{\Phi}^{\nu}$ by using the time step $\Delta t = \mathrm{CFL} * \Delta x/\rho^{\nu}_{\max}$, where $\rho^{\nu}_{\max}$ is an estimate of the maximal characteristic velocity for $\boldsymbol{\Phi}^{\nu}$.

3.4. **Flux vector splittings and viscosity coefficients.** As mentioned before, a flux splitting of the type $f = f^+ + f^-$ with $f^+_u > 0$ and $f^-_u < 0$ is required when the flux function is nonlinear. A standard recipe is provided by the Lax-Friedrichs flux vector splitting,

$$f^+(u) = \frac{1}{2}(f(u) + \alpha u), \qquad f^-(u) = \frac{1}{2}(f(u) - \alpha u) \tag{3.7}$$

where the viscosity coefficient α has to verify that all eigenvalues of $f_u + \alpha I$ are ≥ 0 and all eigenvalues of $f_u - \alpha I$ are ≤ 0. Obviously, a choice such as

$$\alpha = \max_{j=0,\ldots,M-1} \max_{1\leq k\leq N} \big|\lambda^k_j\big|, \tag{3.8}$$

guarantees these inequalities, and we remark that α above can be easily computed for the polydisperse models being studied, since the necessary eigenvalues can be computed in an efficient manner by applying a root finder. However, we can readily apply the results in Lemmas 2.1 and 2.2 in order to provide an estimate for (3.8) which does not require the computation of the eigenvalues, and is 'optimal', in the sense specified in [45],

$$\alpha = \max_{j=0,\ldots,M-1} \max\left\{ \left| v_1\big(\Phi_j\big) + \sum_{k=1}^{N} \gamma_k\big(\Phi_j\big) \right|, \big|v_N\big(\Phi_j\big)\big| \right\}. \tag{3.9}$$

The choice of the viscosity coefficients (3.8) and (3.9) is *global*, hence it can be used at each cell interface, however, the resulting schemes tend to be too dissipative, even when using a characteristic-wise high resolution shock capturing scheme (see the results in [16]). In order to reduce the dissipation effects associated to the global choice of viscosity coefficient described above, a Local Lax Friedrichs (LLF) approach was proposed in [38]. The original viscosity coefficient for the computation of the numerical flux at the $i + 1/2$ interface by the LLF flux splitting approach is given in [38] by

$$\alpha^k_{j+1/2} = \max_{\Phi\in\Gamma} \big|\lambda_k(\Phi)\big|, \quad k = 1, \ldots, N, \tag{3.10}$$

where $\Gamma := \Gamma(\Phi_j, \Phi_{j+1}) \subset \mathbb{R}^N$ is a path in phase space connecting Φ_j and Φ_{j+1}, for example a straight line. Since the characteristic fields are neither genuinely nonlinear nor linearly degenerate, the standard choice

$$\alpha^k_{j+1/2} = \max\big\{\big|\lambda_k(\Phi_j)\big|, \big|\lambda_k(\Phi_{j+1})\big|\big\}. \tag{3.11}$$

will not be appropriate. Indeed, in the numerical experiments section we shall see that (3.11) produces numerical oscillations which do not disappear upon mesh refinement. Hence, the extrema of $\lambda_k(\Phi)$ over Γ in (3.10) needs to be computed. Since there is no closed form for the eigenvalues, this is not an easy task. However, we notice that the interlacing property (2.18) implies that

$$\max_{\Phi\in\Gamma}\big|\lambda_k(\Phi)\big| \le \max_{\Phi\in\Gamma}\big\{\big|v_{k-1}(\Phi)\big|,\big|v_k(\Phi)\big|\big\},\quad k=1,\dots,N, \tag{3.12}$$

where we set $v_0 := M_1$. Let us consider Γ as the straight line joining Φ_j and Φ_{j+1}, the minimum and the maximum of

$$g_k(a) := v_k\big(a\Phi_j + (1-a)\Phi_{j+1}\big),\quad a\in[0,1],$$

for each value of $k\in\{1,\dots,N\}$ can be computed as the minimum or maximum of the extremal set

$$\mathcal{E}_k(\Phi_j,\Phi_{j+1}) := \big\{g_k(0), g_k(1)\big\}\cup\big\{g_k(a) : g_k'(a)=0, a\in(0,1)\big\}. \tag{3.13}$$

For the MLB model, we obtain

$$a = a_k = \frac{(n-1)(d_k^2 - \mathbf{d}_2^{\mathrm{T}}(\Phi_{j+1}))(p_j-p_{j+1}) + (1-p_{j+1})\mathbf{d}_2^{\mathrm{T}}(\Phi_j-\Phi_{j+1})}{n(p_j-p_{j+1})\mathbf{d}_2^{\mathrm{T}}(\Phi_j-\Phi_{j+1})}, \tag{3.14}$$

where p_j is the value of $p=\phi$ associated with node j.

For the modified HS model we have

$$a = a_k = \frac{\phi_{\max}-p_{j+1}}{p_j-p_{j+1}} - \frac{n}{\big(\beta_0+\frac{n}{\phi_{\max}}\big)(p_j-p_{j+1}) + \beta_1 d_k^{-1}\mathbf{d}^{\mathrm{T}}(\Phi_j-\Phi_{j+1}) + \beta_2 d_k^{-2}\mathbf{d}_2^{\mathrm{T}}(\Phi_j-\Phi_{j+1})}. \tag{3.15}$$

Hence, the viscosity coefficient

$$\alpha^k_{j+1/2} = \max_{\Phi\in[\Phi_j,\Phi_{j+1}]}\big\{\big|v_{k-1}(\Phi)\big|,\big|v_k(\Phi)\big|\big\} \tag{3.16}$$

where $[\Phi_j,\Phi_{j+1}]$ denotes the straight line joining Φ_j and Φ_{j+1} can be readily computed at each cell interface. As we shall see in the numerical experiments section, (3.16) provides an adequate recipe for the local viscosity coefficient required by the LLF approach.

3.5. **The SPEC and COMP schemes.** A component-wise WENO5 scheme is defined by the numerical flux

$$\hat f_{j+1/2,k} = \mathcal{R}^+\big(f^+_{j-2,k},\dots,f^+_{j+2,k};x_{j+1/2}\big) + \mathcal{R}^-\big(f^-_{j-1,k},\dots,f^-_{j+3,k};x_{j+1/2}\big), \tag{3.17}$$

where $\mathcal{R}$ is the mapped WENO5 reconstruction operator [26] and $f^\pm_{j,k}$ are given by the global Lax-Friedrichs flux splitting

$$\big(f^\pm_{j,1},\dots,f^\pm_{j,N}\big)^{\mathrm{T}} = \mathbf{f}(\Phi_j)\pm\alpha\Phi_j,\quad j\in\mathbb{Z},$$

with α as defined in (3.9). Notice that this globally defined viscosity coefficient does not require the spectral information of the Jacobian matrix. We remark that the viscosity coefficient relies on the computation of the γ_k coefficients provided in Lemmas 2.1 and 2.2 which is consistent with the observations in [44], about the need to have a proper estimate of the minimal viscosity coefficient given by (3.8).

We use

$$\rho^\nu_{\max} = \max_{j=0,\dots,M-1}\max\left\{\left|v_1\big(\Phi^\nu_j\big)+\sum_{k=1}^N\gamma_k\big(\Phi^\nu_j\big)\right|,\big|v_N\big(\Phi^\nu_j\big)\big|\right\}$$

to estimate the maximal characteristic velocity for $\mathbf{\Phi}^\nu$. The resulting scheme will be referred to as "COMP-GLF".

In order to implement a characteristic-wise scheme, we need the complete eigenstructure of $\mathcal{J}_{\mathbf{f}}(\Phi)$, which is provided by the results of the hyperbolicity analysis summarized in Section 2.4. The normalized left eigenvectors $(\mathbf{l}^k_{j+1/2})^{\mathrm{T}}$ and right eigenvectors $\mathbf{r}^k_{j+1/2}$, $k=1,\dots,N$, of

$$\mathcal{J}_{\mathbf{f}}(\Phi_{j+1/2}),\quad \Phi_{j+1/2} := \frac{1}{2}(\Phi_j+\Phi_{j+1}),$$

are computed using (2.23) and (2.24) for the MLB model and (2.30) for the HS model. The matrices

$$\mathbf{R}_{j+1/2} = \big[\mathbf{r}^1_{j+1/2}, \dots, \mathbf{r}^N_{j+1/2}\big], \qquad \mathbf{R}^{-1}_{j+1/2} = \big[\mathbf{l}^1_{j+1/2}, \dots, \mathbf{l}^N_{j+1/2}\big]^{\mathrm{T}},$$

are needed in order to compute the local characteristic variables and fluxes around the $j+1/2$ interface as follows:

$$g_{j+1/2,i,k} := \big(\mathbf{l}^k_{j+1/2}\big)^{\mathrm{T}}\mathbf{f}(\Phi_{j+i}), \quad g^{\pm}_{j+1/2,i,k} := \frac{1}{2}\big(\mathbf{l}^k_{j+1/2}\big)^{\mathrm{T}}\big(\mathbf{f}(\Phi_{j+i}) \pm \alpha^k_{j+1/2}\Phi_{j+i}\big),$$
$$i = -2, \dots, 3, \quad j \in \mathbb{Z}, \quad k = 1, \dots, N,$$

with $\alpha^k_{j+1/2}$ given by (3.16). For the spectral scheme we compute the numerical fluxes as

$$\hat{\mathbf{f}}_{j+1/2} = \big(\hat{f}_{j+1/2,1}, \dots, \hat{f}_{j+1/2,N}\big)^{\mathrm{T}} = \mathbf{R}_{j+1/2}\hat{\mathbf{g}}_{j+1/2}, \quad j \in \mathbb{Z}, \tag{3.18}$$

where $\hat{\mathbf{g}}_{j+1/2} = (\hat{g}_{j+1/2,1}, \dots, \hat{g}_{j+1/2,N})^{\mathrm{T}}$ is defined as follows. If $\lambda^k_j \cdot \lambda^k_{j+1} \le 0$ (Case 1), we set

$$\hat{g}_{j+1/2,k} = \mathcal{R}^+\big(g^+_{j+1/2,-2,k}, \dots, g^+_{j+1/2,2,k}; x_{j+1/2}\big) + \mathcal{R}^-\big(g^-_{j+1/2,-1,k}, \dots, g^-_{j+1/2,3,k}; x_{j+1/2}\big), \tag{3.19}$$

while for $\lambda^k_j \cdot \lambda^k_{j+1} > 0$ (Case 2), we set

$$\hat{g}_{j+1/2,k} = \begin{cases} \mathcal{R}^+(g_{j+1/2,-2,k}, \dots, g_{j+1/2,2,k}; x_{j+1/2}) & \text{if } \lambda^k_j > 0 \text{ and } \lambda^k_{j+1} > 0, \\ \mathcal{R}^-(g_{j+1/2,-1,k}, \dots, g_{j+1/2,3,k}; x_{j+1/2}) & \text{if } \lambda^k_j < 0 \text{ and } \lambda^k_{j+1} < 0, \end{cases} \quad k = 1, \dots, N. \tag{3.20}$$

We estimate the maximal characteristic velocity for $\mathbf{\Phi}^\nu$ by:

$$\rho^\nu_{\max} = \max_{j=0,\dots,M-1}\max_{k=1,\dots,N}\big|\lambda_k\big(\Phi^\nu_{j+1/2}\big)\big|.$$

In what follows, we will address by "SPEC-INT" the characteristic-wise mapped fifth-order WENO scheme whose numerical fluxes are calculated by (3.18)–(3.20), and where the viscosity coefficient is calculated by (3.16) based on the interlacing property. Alternatively, for comparison purposes we will in one case employ the same scheme with the viscosity coefficient given by the usual choice (3.11) (instead of (3.16)). This scheme will be referred to as "SPEC-LLF".

4. Numerical results

In this section we perform a series of numerical experiments to highlight the numerical issues brought up earlier in the paper. In particular, we shall see that characteristic based WENO schemes are indeed more robust that their component-wise counterparts, and that the choice of viscosity is important in the overall performance of the scheme: an incorrect choice of the viscosity coefficient in the splitting strategy can lead to an oscillatory behavior that remains under mesh refinement. In this section, we take CFL = 0.5 for all examples with two species and CFL = 0.2 for $N = 4, 11$.

4.1. **Example 1 (MLB model, $N = 2$).** The first example [13, 36] corresponds to two species with density $\varrho_{\mathrm{s}} = 2790\,\mathrm{kg/m^3}$ and different diameters $D_1 = 4.96 \times 10^{-4}\,\mathrm{m}$ and $D_2 = 1.25 \times 10^{-4}\,\mathrm{m}$, corresponding to $d_1 = 1$ and $d_2 = D_2/D_1 = 0.25202$. The (unnormalized) depth of the vessel in the original experiment [36] is $L = 0.3\,\mathrm{m}$. The maximum total concentration is $\phi_{\max} = 0.68$, and the initial concentrations are $\Phi^0 = (\phi^0_1, \phi^0_2) = (0.2, 0.05)^{\mathrm{T}}$. The hindered settling factor $V(\phi)$ is chosen according to (2.4) with the exponent $n = 4.7$. The remaining parameters are $g = 9.81\,\mathrm{m/s^2}$, $\mu_{\mathrm{f}} = 0.02416\,\mathrm{Pa\,s}$ and $\varrho_{\mathrm{f}} = 1208\,\mathrm{kg/m^3}$. Moreover, here and in the following examples, the spatial coordinate x refers to normalized depth, and varies between $x = 0$ (meniscus of the suspension) and $x = 1$ (bottom of the settling column). The solution of Example 1 is well known, and has been used as a test case for a variety of methods (see, e.g., [6, 9, 10, 13]).

To compare the performance of SPEC-INT with that of COMP-GLF, we calculate numerical solutions for a sequence of spatial discretizations $\Delta x = 1/M$, and compare the solutions with two alternative reference solutions that have been computed with $M = M_{\mathrm{ref}} = 6400$ and $M = M_{\mathrm{ref}} = 25600$ by SPEC-INT and COMP-GLF, respectively. These solutions are shown in Figures 1 and 2 for the simulated times $t = 50\,\mathrm{s}$ and $t = 300\,\mathrm{s}$, respectively. In Table 1 we show approximate L^1 errors for both schemes at two selected times. These approximate errors are computed as follows. Let us denote by $\phi^M_i(\cdot, t)$ and $\phi^{\mathrm{ref}}_i(\cdot, t)$ denote the numerical solution

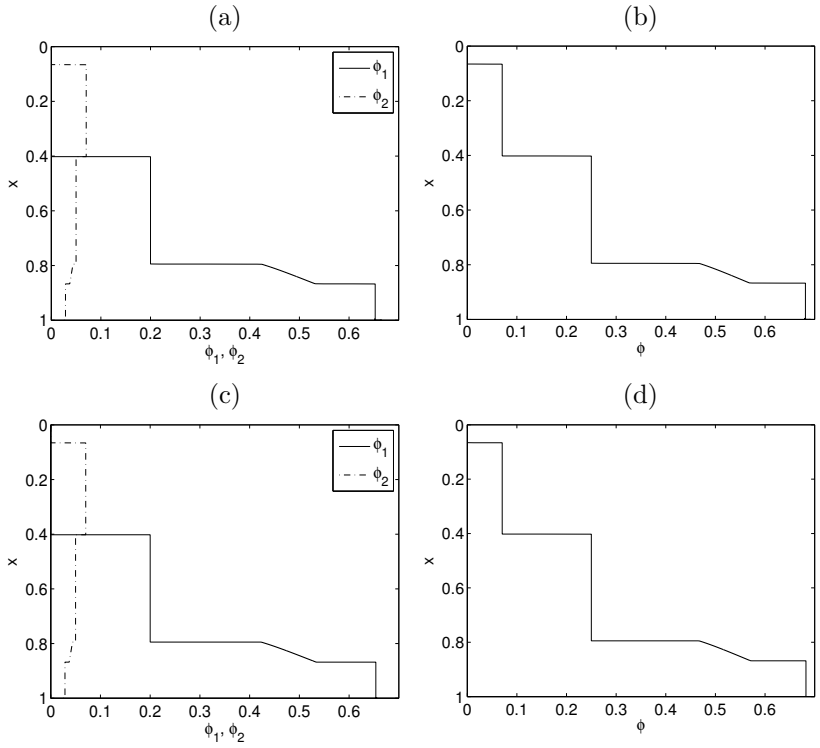

FIGURE 1. Example 1: numerical solution for ϕ_1, ϕ_2 (a, c) and ϕ (b, d) at $t = 50\,\mathrm{s}$ computed by SPEC-INT with $M = 6400$ (a, b) and COMP-GLF with $M = 25600$ (c, d).

M	e_1	cr	e_2	cr	e_{tot}	cr	e_1	cr	e_2	cr	e_{tot}	cr
	SPEC-INT, $t = 50\,\mathrm{s}$						SPEC-INT, $t = 300\,\mathrm{s}$					
100	126.04	-	22.41	-	131.10	-	121.20	-	204.41	-	113.24	-
200	63.37	0.992	10.62	1.077	64.72	1.018	65.40	0.890	107.38	0.929	56.80	0.995
400	30.54	1.053	5.42	0.970	31.60	1.035	33.76	0.954	55.53	0.951	30.07	0.918
800	16.03	0.930	2.62	1.051	16.35	0.950	14.94	1.177	26.79	1.052	15.75	0.932
1600	6.94	1.207	1.21	1.113	7.19	1.185	7.71	0.953	12.99	1.045	7.10	1.149
	COMP-GLF, $t = 50\,\mathrm{s}$						COMP-GLF, $t = 300\,\mathrm{s}$					
100	169.64	-	43.37	-	187.63	-	175.79	-	530.19	-	423.23	-
200	87.06	0.962	20.52	1.080	94.26	0.993	86.40	1.025	255.21	1.055	219.27	0.949
400	44.76	0.960	9.69	1.082	47.56	0.987	45.40	0.928	186.98	0.449	174.58	0.329
800	23.94	0.903	4.82	1.009	25.10	0.923	33.31	0.447	64.09	1.545	54.82	1.671
1600	13.18	0.860	2.41	0.998	13.60	0.884	25.05	0.411	53.33	0.265	43.67	0.328

TABLE 1. Example 1: approximate L^1 errors ($\times 10^{-5}$) and convergence rates (cr). The reference solution is computed by SPEC-INT with $M = 6400$.

for the i-th component at time t calculated for the discretization $M \in \{100, 200, 400, 800, 1600\}$ and the reference discretization M_{ref}, respectively ($M_{\mathrm{ref}} = 6400$ and $M_{\mathrm{ref}} = 25600$ for the SPEC-INT and COMP-GLF schemes, respectively). Assume that $\phi_i^M(x,t) = \phi_{j,i}^M(t) = \text{const.}$ for $x \in [(j-1/2)\Delta x, (j+1/2)\Delta x)$; assume, moreover, that $\phi_i^{\mathrm{ref}}(\cdot, t)$ is piecewise constant on the mesh with meshwidth $1/M_{\mathrm{ref}}$. For a given time t and

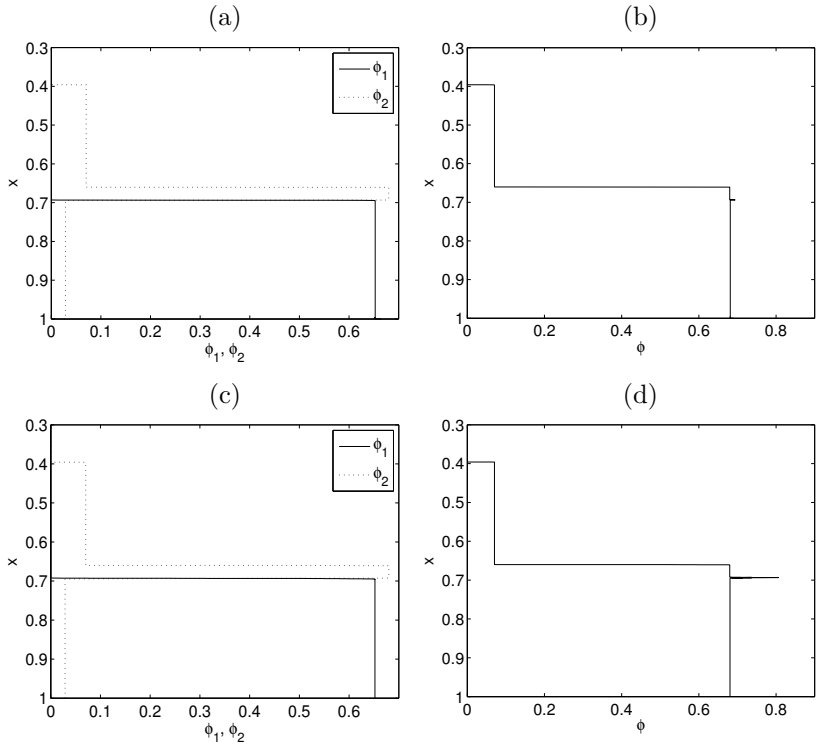

FIGURE 2. Example 1: numerical solution for ϕ_1, ϕ_2 (a, c) and ϕ (b, d) at $t = 300\,\mathrm{s}$ computed by SPEC-INT with $M = 6400$ (a, b) and COMP-GLF with $M = 25600$ (c, d).

M	e_1	cr	e_2	cr	e_{tot}	cr	e_1	cr	e_2	cr	e_{tot}	cr
	SPEC-INT, $t = 50\,\mathrm{s}$						SPEC-INT, $t = 300\,\mathrm{s}$					
100	125.15	-	22.40	-	131.11	-	115.13	-	195.99	-	110.08	-
200	64.58	0.954	10.77	1.056	66.36	0.982	66.21	0.798	102.20	0.939	58.07	0.923
400	33.81	0.934	5.76	0.902	34.94	0.926	33.87	0.967	48.62	1.072	33.25	0.804
800	20.63	0.713	3.03	0.927	20.74	0.752	21.04	0.687	25.26	0.945	21.64	0.620
1600	13.98	0.561	1.82	0.737	13.85	0.582	15.34	0.456	13.64	0.889	15.97	0.439
	COMP-GLF, $t = 50\,\mathrm{s}$						COMP-GLF, $t = 300\,\mathrm{s}$					
100	167.08	-	43.21	-	188.63	-	166.51	-	519.44	-	416.07	-
200	87.17	0.939	20.62	1.067	96.30	0.970	78.01	1.094	243.39	1.094	211.38	0.977
400	47.05	0.890	9.96	1.051	50.80	0.923	33.50	1.220	178.31	0.449	169.73	0.317
800	28.93	0.702	5.25	0.922	30.39	0.741	22.18	0.594	56.16	1.667	49.53	1.777
1600	21.40	0.435	3.10	0.761	21.65	0.489	12.30	0.851	43.48	0.369	36.55	0.439

TABLE 2. Example 1: approximate L^1 errors ($\times 10^{-5}$) and convergence rates (cr). The reference solution is computed by COMP-GLF with $M = 25600$.

$r := M_{\mathrm{ref}}/M \in \mathbb{N}$ we then calculate the approximate L^1 error in species i by

$$e_i = e_i(t) = \left\|\phi_i^{\mathrm{ref}}(\cdot,t) - \phi_i^M(\cdot,t)\right\|_1 = \frac{1}{M_{\mathrm{ref}}} \sum_{j=0}^{M_{\mathrm{ref}}-1} \left|\phi_{j,i}^{\mathrm{ref}}(t) - \phi_{\lfloor j/r \rfloor,i}^{M}(t)\right|, \quad i = 1,\ldots,N.$$

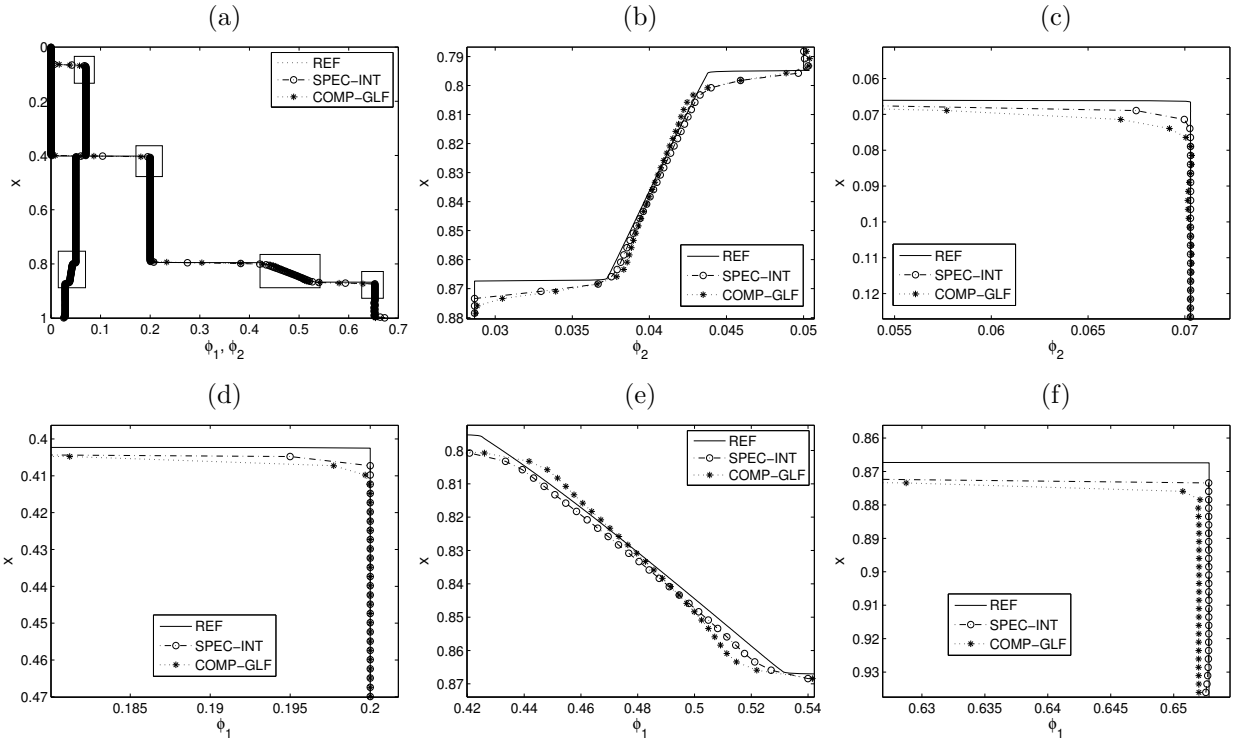

FIGURE 3. Example 1: numerical solution at $t = 50\,\mathrm{s}$ with $M = 400$ (a) and enlarged views (b–f). The reference solution is computed by SPEC-INT with $M = 6400$.

If we define $\phi_j^M(t) := \phi_{j,1}^M(t) + \cdots + \phi_{j,N}^M(t)$ (and analogously, $\phi_j^{\mathrm{ref}}(t)$), then the total approximate L^1 error at that time is given by

$$e_{\mathrm{tot}} = e_{\mathrm{tot}}(t) = \frac{1}{M_{\mathrm{ref}}} \sum_{j=0}^{M_{\mathrm{ref}}-1} \left|\phi_j^{\mathrm{ref}}(t) - \phi_{\lfloor j/r \rfloor}^M(t)\right|.$$

Note that $e_{\mathrm{tot}}(t) \le e_1(t) + \cdots + e_N(t)$.

Table 1 shows that SPEC-INT produces smaller values of the error than COMP-GLF, with respect to its 'converged' solution. The difference is significant in the case of species 2 at $t = 50\,\mathrm{s}$. In the plot of the complete solutions in Figure 3 (a), no difference between both solutions becomes apparent, so we present enlarged views of portions of the numerical simulation (Figures 3 (b–f)) in which the greater accuracy of the solutions generated by SPEC-INT is appreciable. Plot (a) of Figure 4, which corresponds to $t = 300\,\mathrm{s}$, shows the difference of behaviour of both solutions even without the necessity to enlarge the view; nevertheless we present in Figure 4 (b–d) enlarged views to make local differences clearly visible. In Table 1 the reference solution is computed by SPEC-INT with $M_{\mathrm{ref}} = 6400$. To exclude that our conclusion of superiority of SPEC-INT is based on a bias due to the choice of this scheme for the reference solution, we present a second table of errors for this example, Table 2, in which the numerical solutions for $M = 100, \ldots, 1600$ are the same as in Table 1, but we utilize a reference solution obtained by COMP-GLF with $M_{\mathrm{ref}} = 25600$. As a general observation, throughout a rather extense testing process, we may say that a numerical solution obtained by COMP-GLF agrees in quality and resolution power with the solution obtained by SPEC-INT if the meshwidth for COMP-GLF is roughly a fourth of the one used for SPEC-INT.

Of course, for a given value of M the COMP-GLF scheme is faster than the SPEC-INT scheme, since COMP-GLF does not require the complete spectral information, which avoids many computations. Nevertheless, if we seek a fixed level of resolution in the numerical simulation, then SPEC-INT turns out to be

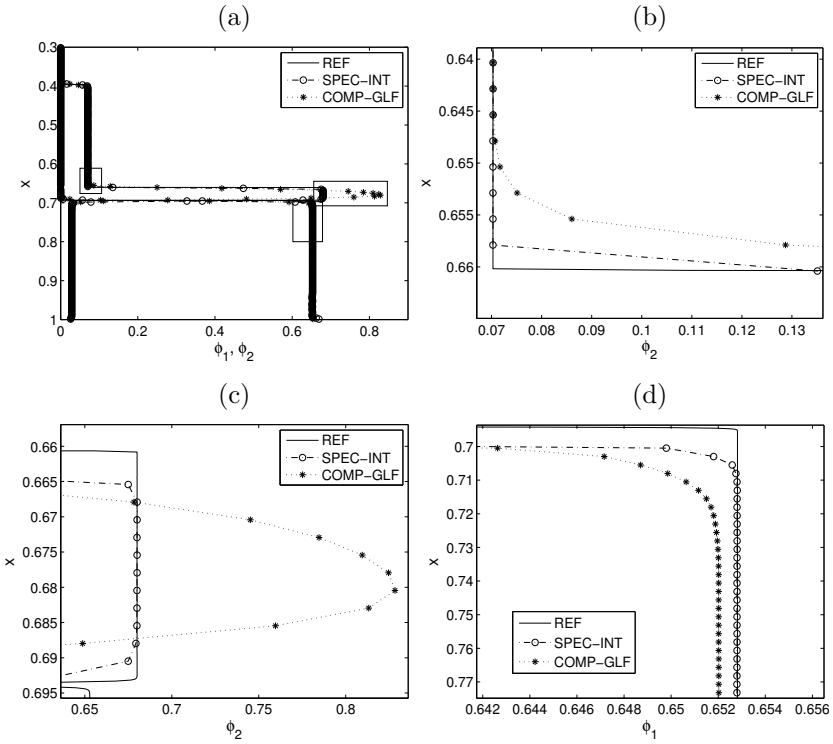

FIGURE 4. Example 1: numerical solution at $t = 300\,\mathrm{s}$ with $M = 400$ (a) and enlarged views (b–f). The reference solution is computed by SPEC-INT with $M = 6400$.

	SPEC-INT, $t = 50\,\mathrm{s}$		SPEC-INT, $t = 300\,\mathrm{s}$		COMP-GLF, $t = 50\,\mathrm{s}$		COMP-GLF, $t = 300\,\mathrm{s}$	
M	e_{tot}	cr	e_{tot}	cr	e_{tot}	cr	e_{tot}	cr
100	103.45	-	158.14	-	200.42	-	212.03	-
200	53.68	0.946	72.64	1.122	104.16	0.944	122.90	0.787
400	23.81	1.173	33.95	1.097	50.07	1.057	79.54	0.628
800	11.95	0.995	12.08	1.491	25.02	1.001	40.90	0.959
1600	5.29	1.174	7.08	0.771	12.13	1.044	23.54	0.797

TABLE 3. Example 2: approximate L^1-errors ($\times 10^{-5}$) and convergence rates (cr).

computationally more efficient. For instance, in Example 1 the CPU time is 21.01 s and 87.15 s for providing the solutions at the respective simulated times $t = 50\,\mathrm{s}$ and $t = 300\,\mathrm{s}$, respectively, with SPEC-INT and $M = 400$, while to obtain a numerical solution of comparable quality (smallness of errors) by COMP-GLF we need to use $M = 1600$ points, and the corresponding CPU times are 29.15 s for $t = 50\,\mathrm{s}$ and 160.80 s for $t = 300\,\mathrm{s}$.

4.2. **Example 2 (MLB model, $N = 4$).** We consider $d_1 = 1$, $d_2 = 0.8$, $d_3 = 0.6$ and $d_4 = 0.4$, $\phi_{\max} = 0.6$, and $\phi_i^0 = 0.05$ for $i = 1, \ldots, 4$. The other parameters are the same as in Example 1. This example goes back to Greenspan and Ungarish [22], and was solved numerically in [8] with the slightly different hindered settling factor $V(\phi) = (1 - (5/3)\phi)^{2.7}$ in [8]. Figures 5 (a, b) and 6 (a, b) display the reference solution obtained with SPEC-INT and $M_{\mathrm{ref}} = 6400$ for $t = 50\,\mathrm{s}$ and $t = 300\,\mathrm{s}$ respectively, while plots (c–f) of both figures are enlarged views of the corresponding numerical solutions obtained with SPEC-INT and COMP-GLF with $M = 400$. Both series of plots show that at $M = 400$ the quality of approximation of piecewise

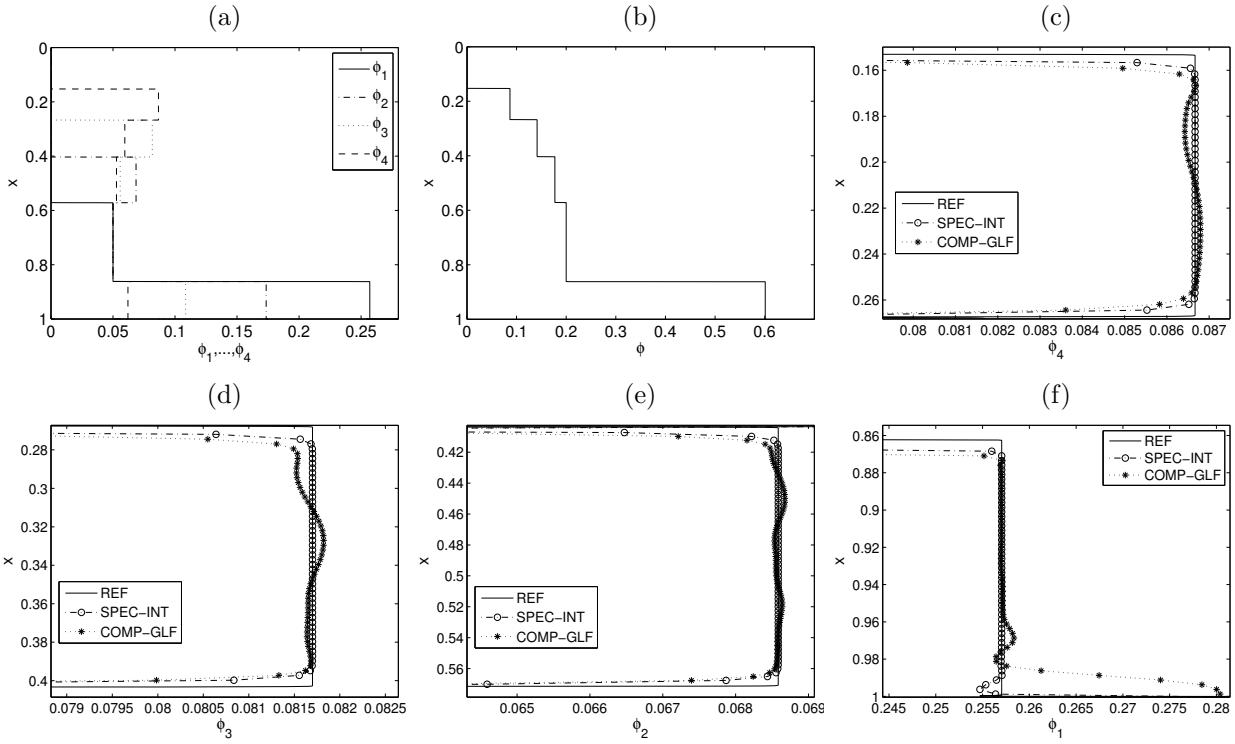

FIGURE 5. Example 2: reference solution for $\phi_1, \ldots, \phi_4$ and ϕ computed by SPEC-INT with $M_{\text{ref}} = 6400$ (a, b), and details of numerical solutions with $M = 400$ (c–f), at $t = 50\,\text{s}$.

i	1	2	3	4	5	6	7	8	9	10	11
$\phi_i^0[10^{-3}]$	0.435	3.747	14.420	32.603	47.912	47.762	32.663	15.104	4.511	0.783	0.060
$D_i[10^{-5}\text{m}]$	8.769	8.345	7.921	7.497	7.073	6.649	6.225	5.801	5.377	4.953	4.529
d_i	1.000	0.952	0.903	0.855	0.807	0.758	0.710	0.662	0.613	0.565	0.516

TABLE 4. Example 3: initial concentrations ϕ_i^0, real and normalized particle sizes D_i and d_i.

constant portions of the solution and the resolution of kinematic shocks by SPEC-INT is superior to that of COMP-GLF. Table 3 displays the approximate total L^1 error and convergence rates for this case. For the times considered the average convergence rate using the SPEC-INT method is close to one. On the other hand, as time increases, the errors increase considerably.

We select this case to compare the performance of SPEC-INT with that of SPEC-LLF, the method based on the simpler viscosity coefficient (3.11). Both choices approximate the same solution globally (not shown here), and a few enlarged views of relevant parts of the numerical solution shown in Figure 7 indicate that the resolution of kinematic shocks by SPEC-LLF is even slightly better than by SPEC-INT. However, we observe spurious oscillations produced by SPEC-LLF in the piecewise constant parts of the solution. These oscillations do not disappear upon mesh refinement, and indicate that the amount of viscosity introduced by (3.11) is not appropriate and possibly insufficient.

4.3. **Example 3 (MLB model, $N = 11$).** This example is based on experimental data from [37], where the settling of a suspension in a column of height $L = 0.935\,\text{m}$ was considered. The initial concentrations ϕ_i^0, diameters D_i and normalized diameters $d_i = D_i/D_1$ are given in Table 4; the maximum total concentration is $\phi_{\max} = 0.641$ [37]. Figures 8 (a) and (b) show the concentration profiles of the reference solution, obtained

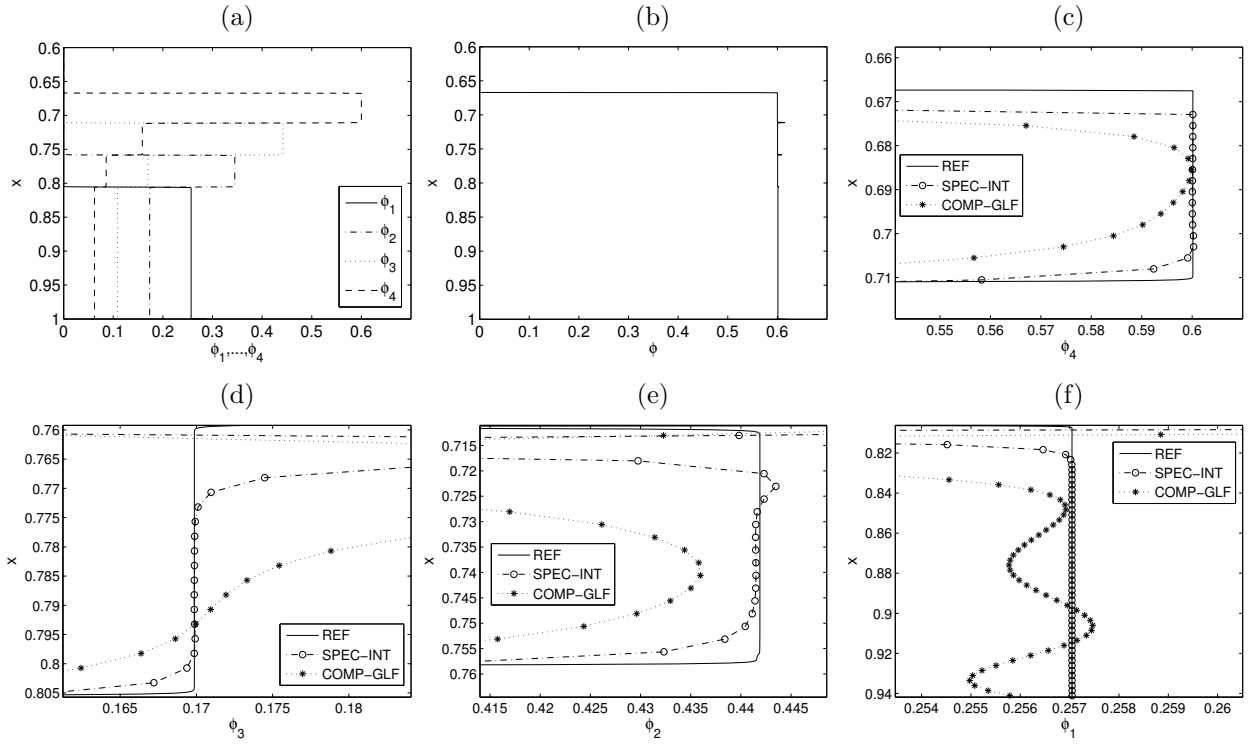

FIGURE 6. Example 2: reference solution for $\phi_1, \ldots, \phi_4$ and ϕ computed by SPEC-INT with $M_{\text{ref}} = 6400$ (a, b), and details of numerical solutions with $M = 400$ (c–f), at $t = 300\,\text{s}$.

	SPEC-INT, $t = 50\,\text{s}$		SPEC-INT, $t = 300\,\text{s}$		COMP-GLF, $t = 50\,\text{s}$		COMP-GLF, $t = 300\,\text{s}$	
M	e_{tot}	cr	e_{tot}	cr	e_{tot}	cr	e_{tot}	cr
100	291.87	-	351.60	-	617.68	-	733.96	-
200	135.51	1.107	182.85	0.943	304.39	1.021	393.88	0.898
400	66.22	1.033	96.86	0.917	164.93	0.884	212.10	0.893
800	36.48	0.860	44.93	1.108	89.51	0.882	112.20	0.919
1600	17.74	1.040	21.07	1.093	46.61	0.941	63.38	0.824

TABLE 5. Example 3: approximate L^1 errors ($\times 10^{-5}$) and convergence rates (cr).

by SPEC-INT with $M_{\text{ref}} = 6400$ at $t = 300\,\text{s}$. Figures 8 (c–f) display enlarged views of portions of the SPEC-INT and COMP-GLF solutions with $M = 400$ at the same time. Again, the superiority of the quality of approximation by SPEC-INT becomes apparent. This observation is also confirmed by the errors displayed in Table 5.

4.4. **Example 4 (MLB model, $N = 2$).** We consider the MLB model with $N = 2$ and the same parameters as Example 1, but now start from the initial datum

$$\Phi(x,0) = \begin{cases} 0.15 & \text{if } x \le 0.5,, \\ 0 & \text{if } x > 0.5, \end{cases} \tag{4.1}$$

corresponding to a settling column whose upper half is initially filled with a suspension, which is separated from the lower half by a "membrane", that is removed at $t = 0$. The suspension pouring into the lower

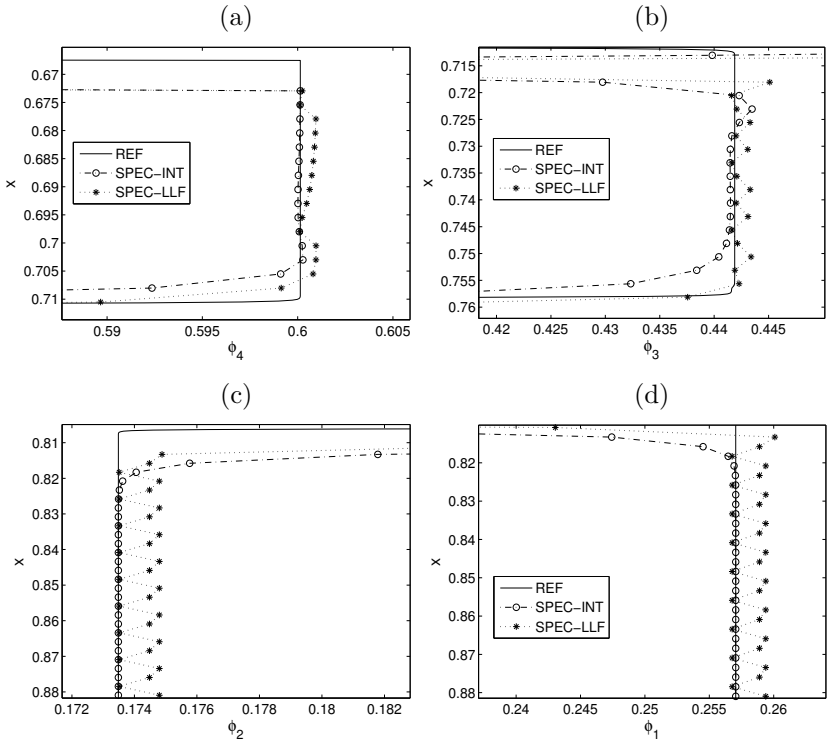

FIGURE 7. Example 2: details of numerical solutions obtained by SPEC-INT and SPEC-LLF with $M = 400$ at $t = 300\,\mathrm{s}$.

M	e_1	cr	e_2	cr	e_{tot}	cr	e_1	cr	e_2	cr	e_{tot}	cr
	SPEC-INT, $t = 50\,\mathrm{s}$						SPEC-INT, $t = 250\,\mathrm{s}$					
100	210.30	-	83.10	-	282.82	-	124.22	-	70.15	-	194.19	-
200	107.67	0.966	34.57	1.265	136.26	1.054	64.25	0.951	29.39	1.255	93.64	1.052
400	66.79	0.689	9.42	1.875	73.25	0.895	55.27	0.217	10.08	1.544	65.35	0.519
800	37.37	0.838	4.53	1.057	40.74	0.846	32.97	0.745	5.55	0.860	38.53	0.762
1600	19.11	0.967	4.29	0.075	22.78	0.838	14.02	1.233	4.04	0.456	18.07	1.092
	COMP-GLF, $t = 50\,\mathrm{s}$						COMP-GLF, $t = 250\,\mathrm{s}$					
100	281.79	-	125.25	-	392.34	-	236.18	-	160.41	-	394.76	-
200	161.65	0.802	73.05	0.778	226.85	0.790	121.40	0.960	77.05	1.058	198.27	0.994
400	88.24	0.873	35.53	1.040	119.74	0.922	73.96	0.715	35.46	1.120	109.42	0.858
800	47.80	0.884	18.30	0.957	64.29	0.897	41.71	0.826	18.30	0.954	60.01	0.866
1600	24.91	0.940	10.47	0.806	34.50	0.898	20.56	1.020	9.84	0.894	30.41	0.980

TABLE 6. Example 4: approximate L^1 errors ($\times 10^{-5}$) and convergence rates (cr) for Riemann problem. The reference solution is computed by SPEC-INT with $M_{\mathrm{ref}} = 6400$.

half will then gradually dilute, and usually a transient rarefaction wave centred at $x = 0.5$ will form. (The rarefaction wave will, however, soon start to interact with concentration information traveling downwards and upwards from the suspension meniscus and column bottom, respectively.) As was shown in [15], this configuration can be realized experimentally (with some effort), and the expanding concentration gradient

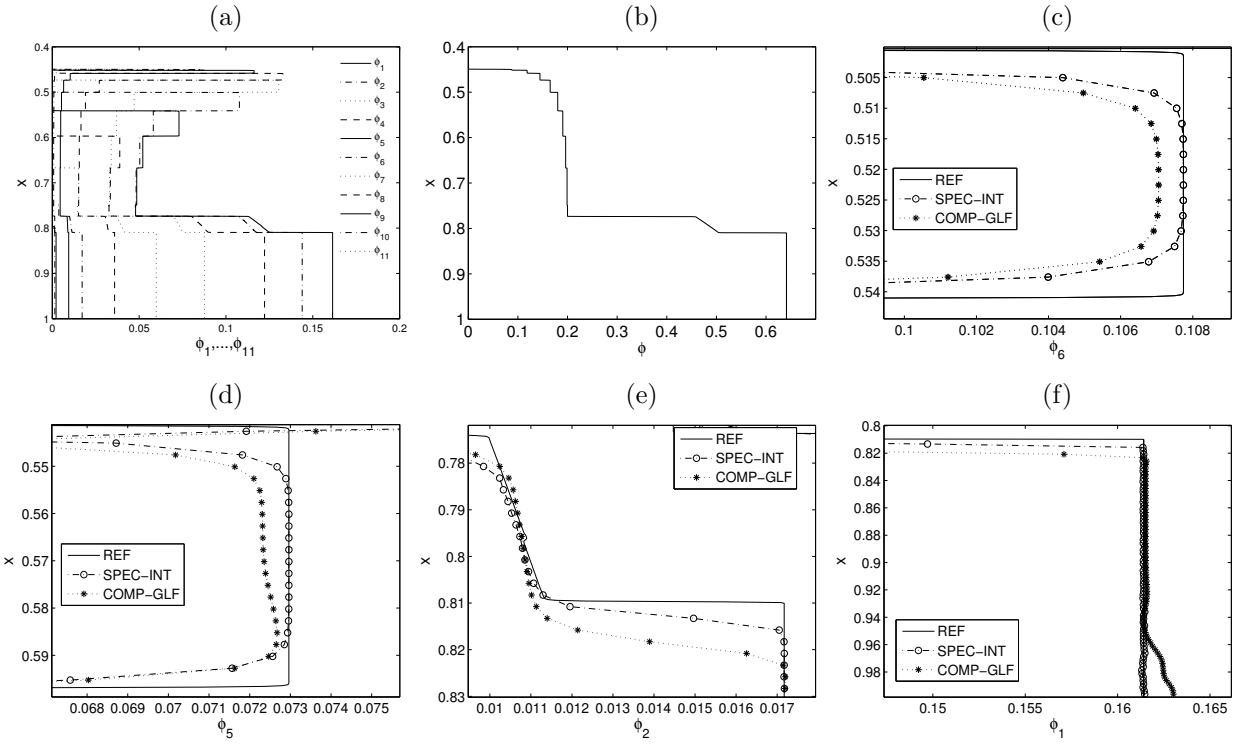

FIGURE 8. Example 3: reference solution for $\phi_1, \ldots, \phi_{11}$ and ϕ computed by SPEC-INT with $M_{\text{ref}} = 6400$ (a, b), and details of numerical solutions with $M = 400$ (c–f), at $t = 300\,\text{s}$.

M	e_1	cr	e_2	cr	e_{tot}	cr	e_1	cr	e_2	cr	e_{tot}	cr
	SPEC-INT, $t = 50\,\text{s}$						SPEC-INT, $t = 250\,\text{s}$					
100	135.94	-	18.45	-	144.90	-	113.12	-	105.16	-	108.60	-
200	70.57	0.946	7.86	1.231	73.50	0.979	59.41	0.929	53.30	0.980	56.05	0.954
400	34.34	1.039	3.76	1.063	35.80	1.038	29.82	0.994	29.01	0.877	27.37	1.034
800	16.49	1.058	1.78	1.073	17.21	1.057	11.26	1.404	12.05	1.267	14.29	0.937
1600	6.71	1.297	0.76	1.226	7.05	1.286	4.86	1.212	5.74	1.068	6.77	1.077
	COMP-GLF, $t = 50\,\text{s}$						COMP-GLF, $t = 250\,\text{s}$					
100	138.48	-	26.99	-	160.72	-	171.39	-	245.80	-	194.93	-
200	70.17	0.981	11.93	1.177	79.71	1.012	86.78	0.982	138.36	0.829	114.99	0.761
400	35.96	0.964	5.31	1.166	40.08	0.992	45.29	0.938	70.90	0.964	56.92	1.014
800	17.02	1.079	2.52	1.072	19.06	1.072	22.87	0.986	39.53	0.843	32.69	0.800
1600	8.39	1.020	1.20	1.073	9.35	1.028	11.40	1.004	22.39	0.820	19.68	0.732

TABLE 7. Example 5: approximate L^1 errors ($\times 10^{-5}$) and convergence rates (cr) for HS model. The reference solution is computed by SPEC-INT with $M_{\text{ref}} = 6400$.

reveals properties of the function $V(\phi)$ which at least for $N = 1$ can be used for flux identification. A similar configuration, but on an unbounded domain, was solved for $N = 2, 4, 8$ and 32 in [11].

Figures 9 and 10, which correspond to the respective simulated times $t = 50\,\text{s}$ and $t = 250\,\text{s}$, show the reference solution obtained by SPEC-INT with $M_{\text{ref}} = 6400$ and details illustrating the difference in

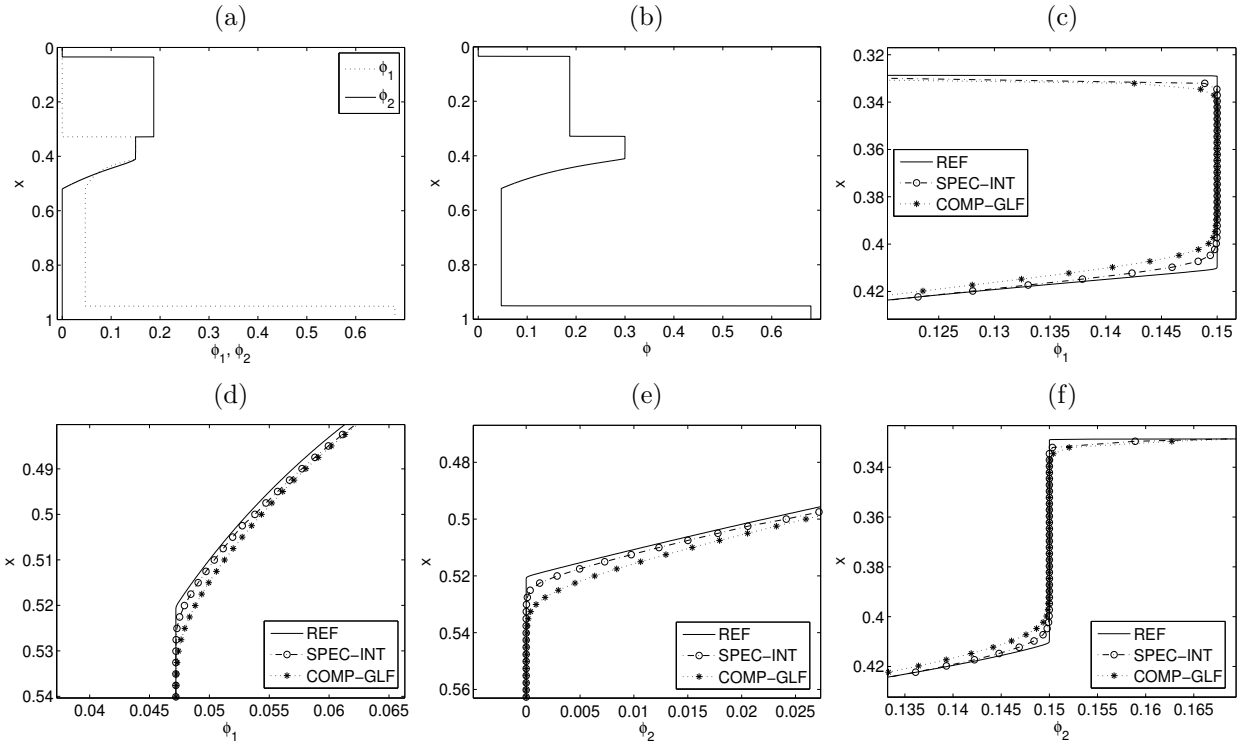

FIGURE 9. Example 4: reference solution for ϕ_1, ϕ_2 and ϕ computed by SPEC-INT with $M_{\text{ref}} = 6400$ (a, b), and details of numerical solutions with $M = 400$ (c–f), at $t = 50\,\text{s}$.

solutions obtained by SPEC-INT and COMP-GLF with $M = 400$. Table 6 displays the errors observed for this example.

4.5. **Examples 5 and 6: HS model with $N = 2$ and $N = 4$.** For these examples we implement the variant of HS model described in Section 2.3. Numerical simulations are shown in Figures 11, 12 ($N = 2$) and 13 ($N = 4$). A noticeable difference with the MLB model (where the flux function is cut abruptly for $\phi \geq \phi_{\max}$) is the profile at the rightmost part of the solution. Table 7 displays the errors observed for Example 5.

5. Conclusions

In this paper we have shown that the implementation of efficient WENO schemes for polydisperse sedimentation models can be accomplished by using the recent hyperbolicity analysis carried out in [9]. In addition, we have been able to characterize the viscosity coefficients to be used in Global-Lax-Friedrichs flux-splitting procedures, as well as in the Local-Lax-Friedrichs flux-splitting procedure. The particular algebraic structure of the velocities of the MLB and HS models permits to exactly determine the extremal set $\mathcal{E}_k(\Phi_j, \Phi_{j+1})$ defined in (3.13), and hence the specific viscosity coefficient to be used at each cell interface.

We have constructed component-wise and characteristic-based WENO5 schemes for two polydisperse sedimentation models, and have compared their performance. As in the case of the MCLWR kinematic traffic models, the characteristic-based schemes, which use the full spectral decomposition of the Jacobian matrix at each cell-interface, are more robust and lead to numerical solutions which are essentially oscillation free. We remark that this situation is absolutely similar to what is observed in the better known case of the Euler equations for gas dynamics simulations, where the superiority of characteristic-based schemes is a well known fact. For gas dynamics, the spectral decomposition of the Jacobian matrix is given in closed

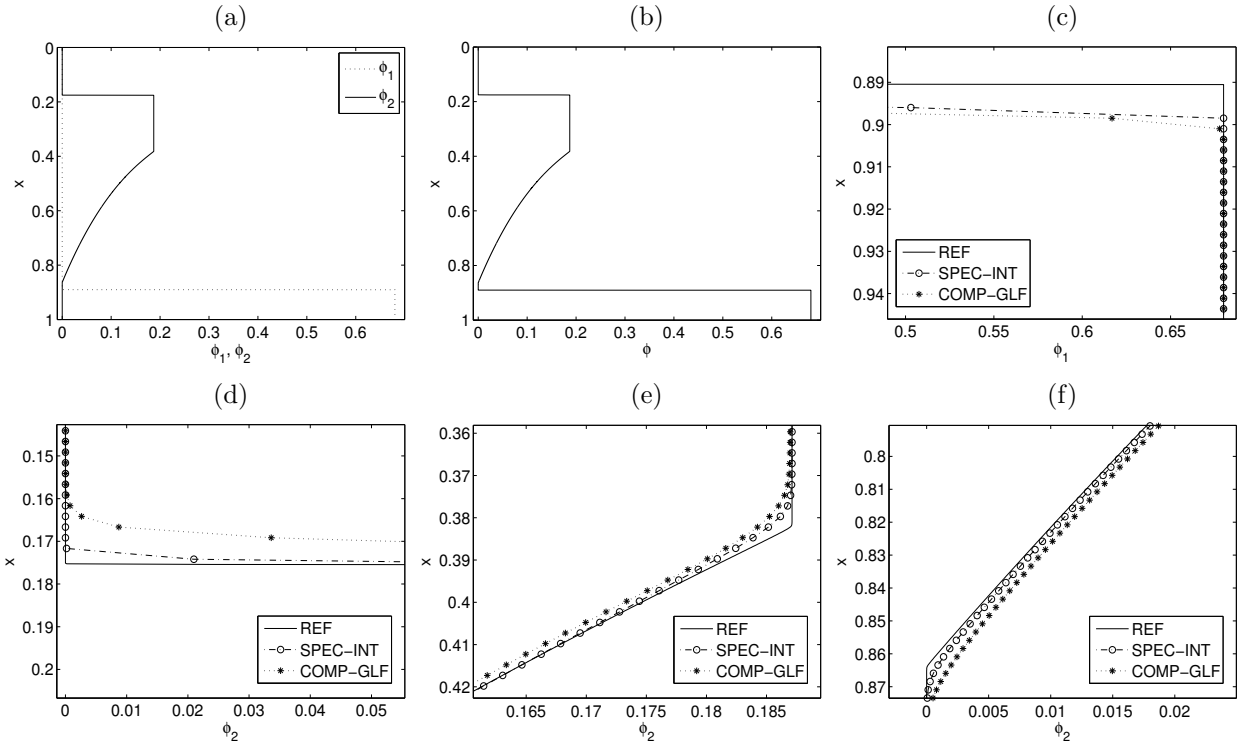

FIGURE 10. Example 4: reference solution for ϕ_1, ϕ_2 and ϕ computed by SPEC-INT with $M_{\text{ref}} = 6400$ (a, b), and details of numerical solutions with $M = 400$ (c–f), at $t = 250\,\text{s}$.

form, hence the use of a characteristic-based scheme poses no special difficulties. For polydisperse models, the spectral decomposition can only be computed numerically. In addition, the characteristic fields are neither genuinely nonlinear nor linearly degenerate, hence the determination of the viscosity coefficients in flux-vector splitting schemes becomes a non-trivial task.

According to the numerical tests shown in this paper, our proposed characteristic-based scheme (SPEC-INT) is very robust, although it is certainly very costly in terms of computational resources, since it involves an intensive usage of the characteristic information. The interlacing property allows other simplifications to be implemented. For example, in Section 3.5, the discrimination between Cases 1 and 2 corresponding to the use of either (3.19) or (3.20) is made in dependence of the sign of the product of eigenvalues $\lambda_j^k \cdot \lambda_{j+1}^k$. The interlacing property (2.18) or (2.19) can be used to compute this sign in terms of velocities rather than eigenvalues.

Nevertheless, we have shown that the SPEC-INT gives a good resolution on the numerical approximation with a relative small number of mesh points, hence it is competitive with respect to the simpler component-wise schemes. We expect the SPEC-INT scheme to be even more competitive than cheaper component-wise schemes, such as COMP-GLF, in an Adaptive Mesh Refinement (AMR) framework, since its non-oscillatory properties will help to avoid unnecessary refinement in regions of constant concentration.

ACKNOWLEDGMENTS

R. Bürger acknowledges partial support by Fondecyt project 1090456, Fondap in Applied Mathematics, project 15000001, BASAL project CMM, Universidad de Chile and Centro de Investigación en Ingeniería Matemática (CI^{2}MA), Universidad de Concepción, and project AMIRA P996/INNOVA 08CM01-17 "Instrumentación y Control de Espesadores". P. Mulet and R. Donat are partially supported by Spanish MCINN

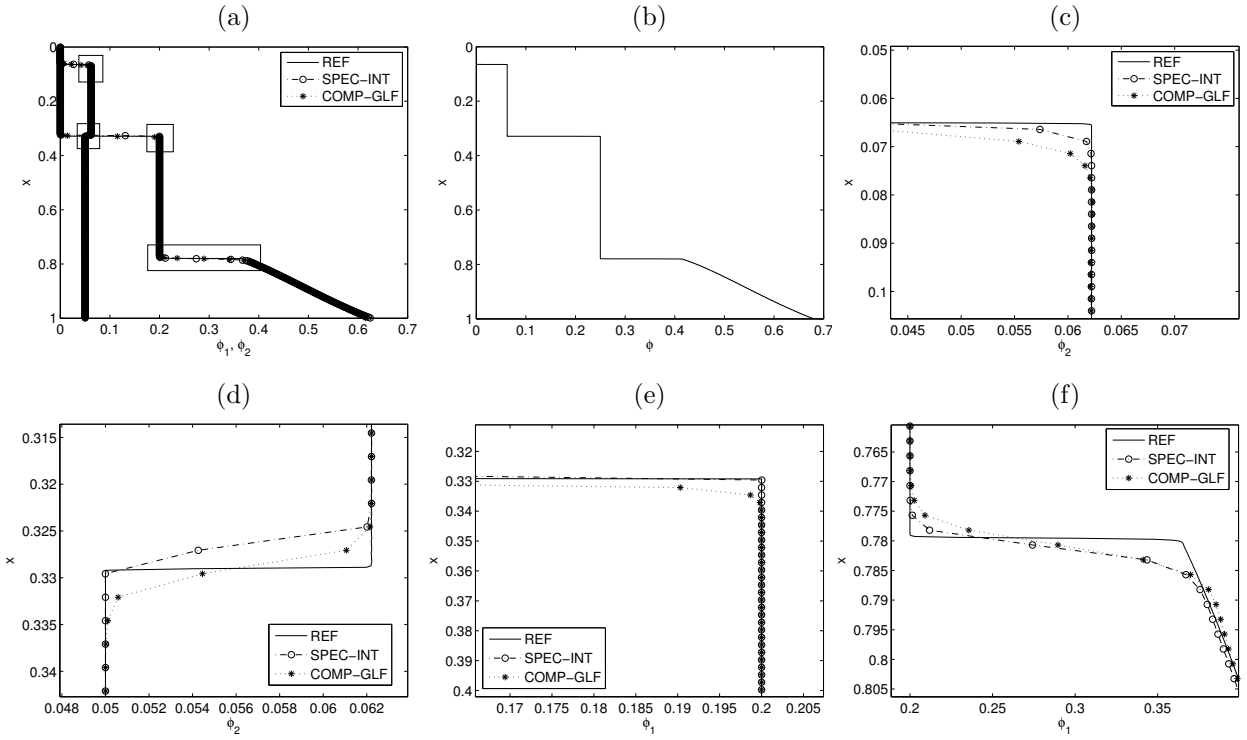

FIGURE 11. Example 5: numerical solution for ϕ_1, ϕ_2 with $M = 400$ (a) and ϕ (b) at $t = 50\,\mathrm{s}$ and enlarged views (c–f) of zones indicated by rectangles in plot (a). The reference solution is computed using SPEC-INT with $M_{\mathrm{ref}} = 6400$.

MTM2008-00974. C. A. Vega acknowledges support by CONICYT fellowship, Universidad del Norte, and MECESUP project UCO0713.

REFERENCES

[1] J. Anderson, A secular equation for the eigenvalues of a diagonal matrix perturbation, Lin. Alg. Appl. 246 (1996) 49–70.
[2] D.K. Basson, S. Berres, R. Bürger, On models of polydisperse sedimentation with particle-size-specific hindered-settling factors, Appl. Math. Modelling 33 (2009) 1815–1835.
[3] G.K. Batchelor, Sedimentation in a dilute polydisperse system of interacting spheres. Part 1. General theory, J. Fluid Mech. 119 (1982) 379–408.
[4] G.K. Batchelor, C.S. Wen, Sedimentation in a dilute polydisperse system of interacting spheres. Part 2. Numerical results, J. Fluid Mech. 124 (1982) 495–528.
[5] S. Benzoni-Gavage, R.M. Colombo, An n-populations model for traffic flow, Eur. J. Appl. Math. 14 (2003) 587–612.
[6] S. Berres, R. Bürger, On Riemann problems and front tracking for a model of sedimentation of polydisperse suspensions, ZAMM Z. Angew. Math. Mech. 87 (2007) 665–691.
[7] S. Berres, R. Bürger, K.H. Karlsen, E.M. Tory, Strongly degenerate parabolic-hyperbolic systems modeling polydisperse sedimentation with compression, SIAM J. Appl. Math. 64 (2003) 41–80.
[8] R. Bürger, F. Concha, K.-K. Fjelde, K.H. Karlsen, Numerical simulation of the settling of polydisperse suspensions of spheres, Powder Technol. 113 (2000) 30–54.
[9] R. Bürger, R. Donat, P. Mulet, C.A. Vega, Hyperbolicity analysis of polydisperse sedimentation models via a secular equation for the flux Jacobian, SIAM J. Appl. Math. 70 (2010) 2186–2213.
[10] R. Bürger, K.-K. Fjelde, K. Höfler, K.H. Karlsen, Central difference solutions of the kinematic model of settling of polydisperse suspensions and three-dimensional particle-scale simulations, J. Engrg. Math. 41 (2001) 167–187.
[11] R. Bürger, A. García, M. Kunik, A generalized kinetic model of sedimentation of polydisperse suspensions with a continuous particle size distribution, Math. Models Methods Appl. Sci. 18 (2008) 1741–1785.
[12] R. Bürger, K.H. Karlsen, E.M. Tory, W.L. Wendland, Model equations and instability regions for the sedimentation of polydisperse suspensions of spheres, ZAMM Z. Angew. Math. Mech. 82 (2002) 699–722.

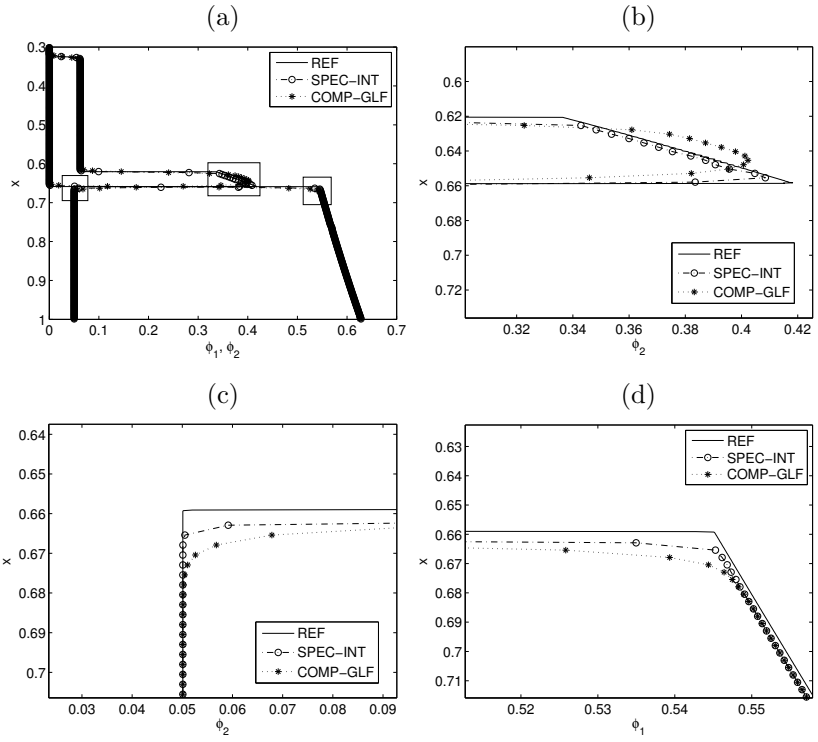

FIGURE 12. Example 5: numerical solution for ϕ_1, ϕ_2 with $M = 400$ (a) at $t = 250\,\mathrm{s}$ and enlarged views (b–d). The reference solution is computed using SPEC-INT with $M_{\mathrm{ref}} = 6400$.

[13] R. Bürger, A. Kozakevicius, Adaptive multiresolution WENO schemes for multi-species kinematic flow models, J. Comput. Phys. 224 (2007) 1190–1222.
[14] R.H. Davis, H. Gecol, Hindered settling function with no empirical parameters for polydisperse suspensions, AIChE J. 40 (1994) 570–575.
[15] S. Diehl, Estimation of the batch-settling flux function for an ideal suspension from only two experiments, Chem. Eng. Sci. 62 (2007) 4589–4601.
[16] R. Donat, P. Mulet, A secular equation for the Jacobian matrix of certain multi-species kinematic flow models, Numer. Methods Partial Differential Equations 26 (2010) 159–175.
[17] R. Donat, P. Mulet, Characteristic-based schemes for multi-class Lighthill-Whitham-Richards traffic models, J. Sci. Comput. 37 (2008) 233–250.
[18] R. Fedkiw, B. Merriman, S. Osher, Simplified upwind discretization of systems of hyperbolic conservation laws containing advection equations, J. Comput. Phys. 157 (2000) 302–326.
[19] S. Gottlieb, D.I. Ketcheson, C.-W. Shu, High order strong stability preserving time discretization, J. Sci. Comput. 38 (2009) 251–289.
[20] S. Gottlieb, C.-W. Shu, Total variation dimishing Runge-Kutta schemes, Math. Comp. 67 (1998) 73–85.
[21] S. Gottlieb, C.-W. Shu, E. Tadmor, Strong stability-preserving high-order time discretization methods, SIAM Rev. 43 (2001) 89–112.
[22] H.P. Greenspan, M. Ungarish, On hindered settling of particles of different sizes, Int. J. Multiphase Flow 8 (1982) 587–604.
[23] K. Höfler, Simulation and modeling of mono- and bidisperse suspensions. Doctoral Thesis, Institut für Computeranwendungen, Universität Stuttgart, Germany, 2000.
[24] K. Höfler, S. Schwarzer, The structure of bidisperse suspensions al low Reynolds numbers. In A.M. Sändig, W. Schiehlen and W.L. Wendland (eds.), Multifield Problems: State of the Art, Springer Verlag, Berlin, 42–49, 2000.
[25] G.S. Jiang, C.-W. Shu, Efficient implementation of weighted ENO schemes, J. Comput. Phys. 126 (1996) 202–228.
[26] A.K. Henrick, T.D. Aslam, J.M. Powers, Mapped weighted essentially non-oscillatory schemes: Achieving optimal order near critical points, J. Comput. Phys. 207 (2005) 542–567.
[27] R.J. LeVeque, Finite Volume Methods for Hyperbolic Problems. Cambridge University Press, Cambridge, UK, 2002.
[28] X.-D. Liu, S. Osher, T. Chan, Weighted essentially non-oscillatory schemes, J. Comput. Phys. 115 (1994) 200–212.

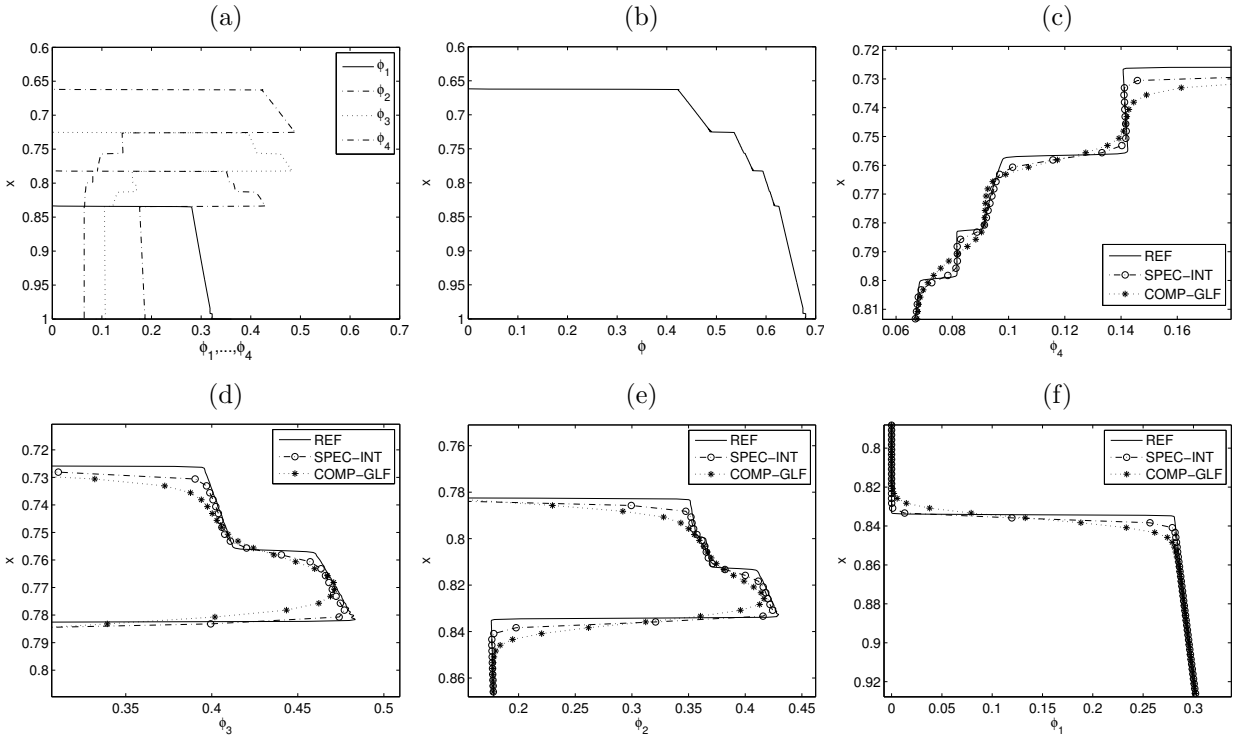

FIGURE 13. Example 6: numerical solution for $\phi_1, \ldots, \phi_4$ with $M = 400$ (a) and ϕ (b) at $t = 250\,\mathrm{s}$ and enlarged views (c–f), where the reference solution is computed using SPEC-INT with $M_{\mathrm{ref}} = 6400$.

[29] M.J. Lockett, K.S. Bassoon, Sedimentation of binary particle mixtures, Powder Technol. 24 (1979) 1–7.

[30] J.H. Masliyah, Hindered settling in a multiple-species particle system, Chem. Eng. Sci. 34 (1979) 1166–1168.

[31] S. Osher, R. Fedkiw, Level Set Methods and Dynamic Implicit Surfaces, Springer, New York, 2003.

[32] A.A.I. Peer, M.Z. Dauhoo, M. Bhuruth, A method for improving the perfomance of the WENO5 scheme near discontinuities, Appl. Math. Lett. 22 (2009) 1730–1733.

[33] F. Rosso, G. Sona, Gravity-driven separation of oil-water dispersions, Adv. Math. Sci. Appl. 11 (2001) 127–151.

[34] S. Ruuth, Global optimization of explicit strong-stability-preserving Runge-Kutta methods, Math. Comput. 75 (2006) 183–207.

[35] S. Ruuth, R. Spiteri, Two barriers on strong-stability-preserving time discretization methods, J. Sci. Comput. 17 (2002) 211–220.

[36] W. Schneider, G. Anestis, U. Schaflinger, Sediment composition due to settling of particles of different sizes, Int. J. Multiphase Flow 11 (1985) 419–423.

[37] P.T. Shannon, E. Stroupe, E.M. Tory. Batch and continuous thickening, Ind. Engrg. Chem. Fund. 2 (1963) 203–211.

[38] C.-W. Shu, S. Osher, Efficient implementation of essentially non-oscilatory shock capturing schemes, J. Comput. Phys. 77 (1988) 439–471.

[39] C.-W. Shu, Essentially non-oscillatory and weighted essentially non-oscillatory schemes for hyperbolic conservation laws. In: B. Cockburn, C. Johnson, C.-W. Shu and E. Tadmor, Advanced Numerical Approximation of Nonlinear Hyperbolic Equations (A. Quarteroni, Ed.), Lecture Notes in Mathematics vol. 1697, Springer-Verlag, Berlin (1998), 325–432.

[40] C.-W. Shu, High order weighted essentially nonoscillatory schemes for convection dominated problems, SIAM Rev. 51 (2009) 82–126.

[41] G.C.K. Wong, S.C. Wong, A multi-class traffic flow model—an extension of LWR model with heterogeneous drivers, Transp. Res. A 36 (2002) 827–841.

[42] M. Zhang, C.-W. Shu, G.C.K. Wong, S.C. Wong, A weighted essentially non-oscillatory numerical scheme for a multi-class Lighthill-Whitham-Richards traffic flow model, J. Comput. Phys. 191 (2003) 639–659.

[43] P. Zhang, R.X. Liu, S.C. Wong, S.Q. Dai, Hyperbolicity and kinematic waves of a class of multi-population partial differential equations, Eur. J. Appl. Math. 17 (2006) 171–200.

[44] P. Zhang, S.C. Wong, S.-Q. Dai, A note on the weighted essentially non-oscillatory numerical scheme for a multi-class Lighthill-Whitham-Richards traffic flow model, Comm. Numer. Meth. Engrg. 25 (2009) 1120–1126.
[45] P. Zhang, S.C. Wong, C.-W. Shu, A weighted essentially non-oscillatory numerical scheme for a multi-class traffic flow model on an inhomogeneous highway, J. Comput. Phys. 212 (2006) 739–756.

Centro de Investigación en Ingeniería Matemática (CI^{2}MA)

PRE-PUBLICACIONES 2010

2010-10 Carlos M. Mora: *Regularity of solutions to quantum master equations: A stochastic approach*

2010-11 Julio Aracena, Luis Gomez, Lilian Salinas: *Limit cycles and update digraphs in Boolean networks*

2010-12 Gabriel N. Gatica, Ricardo Oyarzúa, Francisco J. Sayas: *A residual-based a posteriori error estimator for a fully-mixed formulation of the Stokes-Darcy coupled problem*

2010-13 Lourenco Beirao-Da-Veiga, David Mora, Rodolfo Rodríguez: *Numerical analysis of a locking-free mixed finite element method for a bending moment formulation of Reissner-Mindlin plate model*

2010-14 Fernando Betancourt, Raimund Bürger, Kenneth H. KARLSEN: *A strongly degenerate parabolic aggregation equation*

2010-15 Raimund Bürger, Stefan Diehl, Ingmar Nopens: *A consistent modeling methodology for secondary settling tanks in wastewater treatment*

2010-16 Alfredo Bermúdez, Bibiana López-Rodríguez, Rodolfo Rodríguez, Pilar Salgado: *Numerical solution of transient eddy current problems with input current intensities as boundary data*

2010-17 Rommel Bustinza, Francisco J. Sayas: *Error estimates for an LDG method applied to Signorini type problems*

2010-18 Fabián Flores-Bazán, Fernando Flores-Bazán, Cristian Vera: *A complete characterization of strong duality in nonconvex optimization with a single constraint*

2010-19 Gabriel N. Gatica, Ricardo Oyarzúa, Francisco J. Sayas: *A twofold saddle point approach for the coupling of fluid flow with nonlinear porous media flow*

2010-20 Gabriel N. Gatica, Antonio Marquez, Manuel A. Sanchez: *A priori and a posteriori error analyses of a velocity-pseudostress formulation for a class of quasi-Newtonian Stokes flows*

2010-21 Raimund Bürger, Rosa Donat, Pep Mulet, Carlos A. Vega: *On the implementation of WENO schemes for a class of polydisperse sedimentation models*

Para obtener copias de las Pre-Publicaciones, escribir o llamar a: Director, Centro de Investigación en Ingeniería Matemática, Universidad de Concepción, Casilla 160-C, Concepción, Chile, Tel.: 41-2661324, o bien, visitar la página web del centro: `http://www.ci2ma.udec.cl`







Centro de Investigación en
Ingeniería Matemática (CI²MA)
Universidad de Concepción

Casilla 160-C, Concepción, Chile
Tel.: 56-41-2661324/2661554/2661316
http://www.ci2ma.udec.cl